Geoscientific
Model Development
Discussions

GOLUM-CNP v1.0: a data-driven modeling of carbon, nitrogen and phosphorus cycles in major terrestrial biomes

Yilong Wang[1,*], Philippe Ciais[1], Daniel Goll[1], Yuanyuan Huang[1], Yiqi Luo[2,3,4], Ying-Ping Wang[5], A. Anthony Bloom[6], Grégoire Broquet[1], Jens Hartmann[7], Shushi Peng[8], Josep Penuelas[9,10], Shilong Piao[8,11], Jordi Sardans[9,10], Benjamin D. Stocker[12,13], Rong Wang[14], Sönke Zaehle[15], Sophie Zechmeister-Boltenstern[16]

[1] Laboratoire des Sciences du Climat et de l'Environnement, CEA-CNRS-UVSQ- Université Paris Saclay, Gif-sur-Yvette, France

[2] Center for Ecosystem Science and Society, Northern Arizona University, Flagstaff, AZ, USA

[3] Department of Earth System Science, Tsinghua University, Beijing, China

[4] Department of Microbiology and Plant Biology, University of Oklahoma, Norman, OK, USA

[5] CSIRO Oceans and Atmosphere, PMB #1, Aspendale, Victoria, Australia

[6] Jet Propulsion Laboratory, California Institute of Technology, Pasadena, CA, USA

[7] Institute for Geology, KlimaCampus, Universität Hamburg, Bundesstrasse 55, D-20146 Hamburg, Germany

[8] Sino-French Institute for Earth System Science, College of Urban and Environmental Sciences, Peking University, Beijing, China

[9] CSIC, Global Ecology Unit CREAF-CSIC-UAB, Bellaterra, Catalonia, Spain

[10] CREAF, Cerdanyola del Vallès, Catalonia, Spain

[11] Institute of Tibetan Plateau Research, Chinese Academy of Sciences, Beijing, China

[12] AXA Chair of Biosphere and Climate Impacts, Grand Challenges in Ecosystems and the Environment and Grantham Institute – Climate Change and the Environment, Department of Life Sciences, Imperial College London, Silwood Park Campus, Ascot, UK

[13] Institute for Atmospheric and Climate Science, ETH Zürich, Universitätstrasse 16, Zürich, Switzerland

[14] Department of Global Ecology, Carnegie Institution for Science, Stanford, CA, USA

[15] Max Planck Institute for Biogeochemistry, Jena, Germany

[16] University of Natural Resources and Life Sciences Vienna, Institute of Soil Research, Department of Forest and Soil Sciences, Vienna, Austria

*Corresponding to: Yilong Wang[1] (yilong.wang@lsce.ipsl.fr)

Abstract. Global terrestrial nitrogen (N) and phosphorus (P) cycles are coupled to the global carbon (C) cycle for net primary production (NPP), plant C allocation and decomposition of soil organic matter, but N and P have distinct pathways of inputs and losses. Current C-nutrient models exhibit large uncertainties in their estimates of pool sizes, fluxes and turnover rates of nutrients, due to a lack of consistent global data for evaluating the models. In this study, we present a new model-data fusion framework called Global Observation-based Land-ecosystems Utilization Model of Carbon, Nitrogen and Phosphorus (GOLUM-CNP) that combines the CARbon DAta MOdel fraMework (CARDAMOM) data-constrained C-cycle analysis with spatially explicit data-driven estimates of N and P inputs and losses and with observed stoichiometric ratios. We calculated the steady-state N- and P-pool sizes and fluxes globally for large biomes. Our study showed that new N inputs from biological fixation and deposition supplied >20% of total plant uptake in most forest ecosystems but accounted for smaller fractions in boreal forests and grasslands. New P inputs from atmospheric deposition and rock weathering supplied a much smaller fraction of total plant uptake than new N inputs, indicating that the terrestrial C sink may ultimately be constrained by low P. Nutrient-use efficiency, defined as the ratio of gross primary production (GPP) to plant nutrient uptake, can be diagnosed from our model results and compared between biomes. Tropical forests had the lowest N-use efficiency and the highest P-use efficiency of the forest biomes. An analysis of sensitivity and uncertainty indicated that the NPP-allocation fractions to leaves, roots and

Geoscientific
Model Development
Discussions

1 wood contributed the most to the uncertainties in the estimates of nutrient-use efficiencies. Correcting for biases in NPP-

2 allocation fractions produced more plausible gradients of N- and P-use efficiencies from tropical to boreal ecosystems and

3 highlighted the critical role of accurate measurements of C allocation for understanding the N and P cycles.

4 **1   Introduction**

5   Nitrogen (N) and phosphorus (P) cycling are tightly coupled with the global carbon (C) cycle (Cleveland et al., 2013;

6 Elser et al., 2007; Gruber and Galloway, 2008; Ver et al., 1999) in terrestrial ecosystems. N and P uptake by plants control

7 productivity and growth (Norby et al., 2010; Sutton et al., 2008; Vitousek and Howarth, 1991). N and P also affect soil C by

8 nutrient controls on the mineralization of litter and soil organic matter (Gärdenäs et al., 2011; Melillo et al., 2011). The coupling

9 between the C, N and P cycles affects the projected terrestrial C cycle under climate change and rising atmospheric CO_2,

10 because additional productivity will only be realized if plants can increase their uptake or recycling of nutrients (Hungate et

11 al., 2003; Sun et al., 2017; Wang and Houlton, 2009; Zaehle et al., 2015). The estimates of the magnitudes of these responses

12 of ecosystems in the future, however, are highly uncertain (Peñuelas et al., 2013; Wieder et al., 2015).

13   Nutrients are important for understanding the current perturbation and future projections of the global C cycle, so several

14 land surface models (LSMs) have incorporated terrestrial N cycling (Goll et al., 2012; Medvigy et al., 2009; Parton et al., 2010;

15 Thornton et al., 2007; Wang et al., 2001, 2010; Weng and Luo, 2008; Xu-Ri and Prentice, 2008; Yang et al., 2009; Zaehle et

16 al., 2014; Zaehle and Friend, 2010). Fewer models have incorporated the cycling of P and its interactions with C dynamics

17 (Goll et al., 2012, 2017a; Wang et al., 2010). Many of the underlying processes are not fully understood, and comprehensive

18 data for evaluation are lacking to constrain the representation of some key processes (Zaehle et al., 2014), so model structure,

19 the processes included and the prescribed parameters differ widely among LSMs (Zaehle and Dalmonech, 2011). For example,

20 some models assume constant stoichiometry in plant tissues (Thornton et al., 2007; Weng and Luo, 2008), but others have a

21 flexible stoichiometry (Wang et al., 2010; Xu-Ri and Prentice, 2008; Yang et al., 2009; Zaehle and Friend, 2010). Some models

22 do not include losses of gaseous N due to denitrification (Medvigy et al., 2009), some use the "hole-in-the-pipe" approach to

23 simulate the denitrification flux (Thornton et al., 2007; Wang et al., 2010), assuming it is proportional to net N mineralization,

24 and others calculate this flux as a function of soil N-pool size and soil conditions (temperature, moisture) (Parton et al., 2010;

25 Xu-Ri and Prentice, 2008; Zaehle and Friend, 2010). Furthermore, these models are usually only evaluated for specific

26 ecosystems or at a limited number of sites (Goll et al., 2017a; Yang et al., 2014). The application of these models for

27 simulations with global coverage is thus highly uncertain (Goll et al., 2012; Wang et al., 2010; Zhang et al., 2011). Jahnke

28 (2000) estimated that the global total amount of soil P was 200 Pg and that the P contained in plants was 3 Pg. These estimates,

29 though, were questioned by Wang et al. (2010) and Goll et al. (2012), who estimated that P in plants ranged between 0.23 and

30 0.39 Pg and that P in soil was only 26.5 Pg.

31   A growing number of data sets in recent decades have addressed many aspects of the nutrient cycles and their interactions

32 with C dynamics. For example, Zechmeister-Boltenstern et al. (2015) synthesized the stoichiometry in different ecosystem

33 compartments and highlighted the latitudinal gradients of plant, litter and soil stoichiometry. Liu et al. (2017) evaluated soil

34 net N mineralization among different ecosystems at the global scale and found that net N mineralization decreased with

35 increasing latitude. They also found that the N mineralization at higher latitudes are more sensitive to temperature changes

36 than at lower latitudes, indicating potential alleviation of N limitation for plants' productivity at boreal regions under global

37 warming. Yang et al. (2013) provided spatially explicit estimates of different forms of soil P globally and thus made it possible

38 to assess the P content that is available for plant uptake. These data help to improve the understanding of the global terrestrial

39 biogeochemical cycles across large climatic and ecological gradients and can in principle be combined to provide an integrated

40 analysis of terrestrial C, N and P dynamics. Estimates of C, N and P cycles consistent with all these data sets, however, have

41 not yet been successfully provided due to the difficulties in combining these data sets with different uncertainties and

42 inconsistent spatial/temporal representations.

1   We present a new data-driven modeling framework called Global Observation-based Land-ecosystems Utilization Model

2   of Carbon, Nitrogen and Phosphorus (GOLUM-CNP) for providing observation-based estimates of C, N and P pools and

3   fluxes. We calculated the C, N and P cycles for an assumed steady state corresponding to present-day conditions (see Sect.

4   3.2). Starting from a CARbon DAta MOdel fraMework (CARDAMOM) data-constrained analysis of the terrestrial C cycle

5   (Bloom et al., 2016), which is based on the Data Assimilation Linked Ecosystem Carbon Model version two (DALEC2, Bloom

6   and Williams, 2015; Williams et al., 2005) and on observations of biomass, soil C, leaf area index (LAI) and fire emissions,

7   we incorporated observed stoichiometric ratios (C:N:P) in each pool, N and P external input fluxes, transformations in

8   ecosystems and losses and observation-based information for the fraction of gaseous losses of N to total (gaseous and leaching)

9   losses of N from ^{15}N measurements in soils. We first present the model structure (Sect. 2) and the data sets used to derive its

10   outputs consisting of pools, fluxes and turnovers of C, N and P (Sect. 3). The model results and their sensitivities to the input

11   observation-based data sets are then further analyzed in Sect. 4. Finally, we discuss the potential applications of the framework

12   for model development, calibration and evaluation.

13   **2   Model structure**

14   The GOLUM-CNP framework describes the C, N and P cycles in natural terrestrial ecosystems (Fig. 1). We follow the

15   model structure of DALEC2 and CARDAMOM for the C cycle. Biomass is divided into three pools: foliage, fine roots and

16   wood. The wood pool includes woody stems and coarse roots. The litter pool in Fig. 1 corresponds to fine litter from leaves

17   and fine roots. Soil organic matter (SOM) receives C from fine litter and woody biomass. Two additional pools not present in

18   CARDAMOM are added, representing soil inorganic N and P. These two inorganic N and P pools are assumed to represent

19   nutrients accessible by plants (see Sect. 2.1 and 2.2). Fluxes connecting the pools are described by the differential equations

20   given in Appendices A-C. An overview of the C, N and P cycles and their interactions are presented in the following sections.

21   A full list of the symbols and their definitions is given in Table 1.

22   **2.1 C cycle**

23   The C cycle in the GOLUM-CNP model structure is based on the DALEC2 model (Bloom et al., 2016; Bloom and

24   Williams, 2015). We used a similar structure to define the C pools of GOLUM-CNP but grouped the DALEC2 foliar and labile

25   vegetation C pools into a single foliar pool (Fig. 1). Net primary production (NPP) is allocated to the three biomass pools. The

26   outgoing fluxes from biomass pools include losses from fire, the transfer of foliage and root detritus to litter and the transfer

27   of wood debris directly to the SOM pool. The outgoing fluxes from litter include losses from fire and decomposition. A fraction

28   of decomposed litter is respired and returned to the atmosphere as CO_2, the remaining fraction being converted to SOM. The

29   SOM pool loses C by fire and decomposition. Differential equations governing the dynamics of C pools are given in Appendix

30   A.

31   **2.2 N cycle**

32   The N cycle in GOLUM-CNP is coupled to the C cycle: the pool sizes of N are decided by the C-pool sizes and their

33   respective N:C ratios; the N fluxes from different pools are determined by the N-pool sizes and corresponding turnover rates.

34   The N cycle includes a specific soil inorganic-N pool in addition to the five pools of the C cycle. The inputs of N to ecosystems

35   include atmospheric N deposition and N fixation (N_d+N_{fix} in Fig. 1), both of which are assumed to enter the inorganic-N pool.

36   The total N-fixation flux in this study includes both symbiotic and asymbiotic fixation (see Sect. 3.1), but we do not separate

37   the two processes and assume that they together contribute to the inorganic-N pool, even though N fixation is controlled by

38   plants. N uptake (F_N) by plants is assumed to be solely from the inorganic-N pool. Organic N is an important N supply for

39   plants (Näsholm et al., 2009), especially in boreal-forest and tundra ecosystems (Schimel and Bennett, 2004; Schimel and

40   Chapin, 1996; Zhu and Zhuang, 2013), but the quantitative importance of this process is still unknown for other ecosystems

Geoscientific
Model Development
Discussions

1   globally. We thus ignored the uptake of organic soil N. N uptake by plants from the inorganic-N pool is modeled from the N:C

2   ratio of NPP allocated to biomass pools minus the resorbed N. In the real world, N is only resorbed at the end of the growing

3   season or leaf lifespan and then stored in plant organs and remobilized during the next growing season. Here, because our

4   model does not have a sub-annual time step, rates of resorption described by a resorption coefficient (Appendix B) are assumed

5   to be constant over time. We also assumed that N is not resorbed from fine roots or wood, because evidence for this process is

6   inconclusive (Gordon and Jackson, 2000; Zechmeister-Boltenstern et al., 2015). N mineralization is modeled along with litter

7   and SOM decomposition. N immobilization due to the uptake of inorganic soil N by soil organisms is modeled to match the

8   higher N:C ratio of the SOM pool than its donor (wood and litter) pools. The output of N from ecosystems occurs from fire,

9   denitrification and leaching. The N lost due to fire is assumed to be emitted only in gaseous form, because the proportion of N

10   retained in the residual ash is very small during a fire (Niemeyer et al., 2005; Qian et al., 2009). We consider the gaseous loss

11   of inorganic N from denitrification but ignore the volatilization of NH_4^+ N. This flux usually occurs at a soil pH >8 (Freney et

12   al., 1983) or after application of N fertilizers (Yang et al., 2009), and NH_3 emissions from soils under natural vegetation are

13   relatively small globally (5 Tg N y^{-1}, Bouwman et al., 1997; Houlton et al., 2015), representing <5% of total gaseous loss, so

14   the omission of NH_4^+ N volatilization will not introduce large biases in our model for most regions. The dynamics of N in the

15   pools are summarized by the differential equations in Appendix B.

16   **2.3 P cycle**

17   The P cycle, like the N cycle, is also coupled to the C cycle; the dynamics of P in the pools are depicted by the differential

18   equations in Appendix C. The external inputs of P to ecosystems include atmospheric P deposition and P released from P-

19   bearing minerals by chemical weathering (P_d+P_w in Fig. 1). P from deposition and rock weathering enter the soil inorganic-P

20   pool. The structure of the P cycle is the same as for the N cycle described above for foliar-P resorption, P released from the

21   decomposition of litter and SOM and the immobilization of inorganic soil P by soil organisms. Inorganic P, unlike inorganic

22   N, can be sorbed onto/into soil particles and subsequently become occluded. This form is assumed to be unavailable to plants.

23   We modeled strong sorption with a constant rate. Output pathways of P from the ecosystem include fire, leaching and

24   conversion to strongly sorbed and occluded P. Notably, not all P mobilized by fire is emitted in gaseous form, and some of the

25   P is retained in the residual ash (Niemeyer et al., 2005; Qian et al., 2009). We used a constant fraction of 75% (Niemeyer et

26   al., 2005; Qian et al., 2009) to model the P retained in the residual ash during a fire, and this fraction of P enters the inorganic

27   pool.

28   **3   Methods**

29   **3.1 Input data sets**

30   All parameters used as inputs for the calibration of GOLUM-CNP are listed in Table 1. The variables inferred assuming

31   a steady state are also listed. The estimates of fluxes and C-pool sizes were based on mass balances, and the estimates of N-

32   and P-pool sizes were derived from the C-pool size and stoichiometric data (see below and Appendix E). We used the C fluxes

33   and turnover times of C pools derived from CARDAMOM for the C cycle (Bloom et al., 2016), which offered a data-consistent

34   analysis of terrestrial C cycling on a global 1 °×1 °grid for 2001-2010 by optimizing the DALEC2 model parameters to match

35   the state and process variables with the global observations of MODIS LAI (Myneni et al., 2015), soil C (Hiederer and Köchy,

36   2011), burned area (Giglio et al., 2013) and tropical biomass (Saatchi et al., 2011). Although CARDAMOM data-driven

37   analysis only reported the C pools and fluxes, the impacts of N and P on the C cycle have been implicitly reflected in

38   CARDAMOM through the constraints by some of the observations. For example, the availability of N and/or P limits the

39   growth of vegetation and thus the LAI observed (Klodd et al., 2016; Reich et al., 2010); the N and P contents in soil control

40   the decomposition of soil C and thus the soil C pool observed (Manzoni et al., 2010). In this sense, it is appropriate to use

Geoscientific

Model Development

Discussions

1 CARDAMOM as a basis for the GOLUM-CNP data-driven modeling of C, N and P cycles.

2   The current synthesis of site data for pool stoichiometry was mainly aggregated at the scale of the biomes, so we divided

3 the global vegetation into seven biomes, following Zechmeister-Boltenstern et al. (2015): tropical rainforests (TRF), temperate

4 deciduous forests (TEDF), temperate coniferous forests (TECF), boreal coniferous forests (BOCF), tundra (TUN), tropical/C4

5 grasslands (TRG) and temperate/C3 grasslands (TEG). We used observed biome-averaged values of the N:C ratios of each

6 pool for the seven biomes from the synthesis by Zechmeister-Boltenstern et al. (2015).

7   We used the spatially explicit estimates of N deposition (Wang et al., 2017) and N fixation (both symbiotic and asymbiotic)

8 (Peng et al., submitted) for 2001-2010 for the N inputs, which were constrained by the observation-based estimates of C:N

9 ratios of the various plant pools, soil microbial biomass and organic matter under present conditions. The resorption

10 coefficients of leaves for the seven biomes were derived from the N:C ratios of leaves and leaf litter reported by Zechmeister-

11 Boltenstern et al. (2015). The rate of loss of inorganic N by leaching was determined from data for total soil moisture and

12 runoff (Eq. B7). The spatially explicit estimate of total soil moisture was derived from the European Centre for Medium-Range

13 Weather Forecasts (ECMWF) Interim Reanalysis (ERA-Interim/Land; Albergel et al., 2013; Balsamo et al., 2015). The global

14 gridded estimate of runoff data was obtained from the Global Runoff Data Centre (GRDC, http://www.grdc.sr.unh.edu/), which

15 is constrained by observed river discharges from 663 stations globally. We used observation-based estimates of the fraction of

16 N lost by denitrification to the total inorganic-N loss (denitrification + leaching) pathways (Goll et al., 2017b) to calibrate the

17 denitrification-loss flux. This fraction of denitrification loss (f_{denit}) was derived using a process-based statistical model fitted

18 to global soil δ^{15}N data sets, based on the distinct ^{15}N fractionation effect of denitrification versus loss from leaching (Bai et

19 al., 2012; Houlton and Bai, 2009).

20   We constrained the P cycle using the spatially explicit estimates by Wang et al. (2017) for P deposition for 2001-2010.

21 Spatially explicit estimates of P input from rock weathering were derived from data for river discharge and the chemical

22 composition of minerals by Hartmann et al. (2014). The P:C ratios and resorption coefficients for the seven biomes were

23 obtained from Zechmeister-Boltenstern et al. (2015). Only a fraction of total inorganic P can be lost by leaching, and this

24 fraction of dissolved inorganic P in total labile P was derived based on the observations of Hedley soil P fractions as the resin-

25 extractible P divided by total labile P reported by Yang and Post (2011) for the twelve USDA soil orders. The constant rate at

26 which inorganic P becomes strongly sorbed (f_{sorb}, Eq. C6) was fixed at 0.04 y^{-1} (Goll et al., 2017a).

27   Zechmeister-Boltenstern et al. (2015) only reported the stoichiometric ratios and the N and P resorption coefficients for

28 seven large natural biomes, but other input variables were grid-based products. A land-cover map was used to aggregate the

29 grid-based C-cycle variables from Bloom et al. (2016) into the biomes used by Zechmeister-Boltenstern et al. (2015). The

30 land-cover map was derived from the dominant land-cover type for each grid cell for the globe, excluding croplands, from the

31 land-cover map of the Climate Change Initiative (LC_CCI) established by the European Space Agency (ESA) (Bontemps et

32 al., 2013) at 0.25 °×0.25 ° resolution. Specifically, we used the 2010 map to classify all grid cells into one of the seven natural

33 biomes of Zechmeister-Boltenstern et al. (2015) (Fig. 2), following the methodology presented by Poulter et al. (2015).

34 **3.2 Model integration and output diagnostics**

35   We applied the model framework described in Sect. 2 to derive a data-driven estimate of steady-state C, N and P cycling.

36 A steady state indicates that annual mean input fluxes for all pools are assumed to be balanced by annual mean outgoing fluxes,

37 with the annual mean outgoing fluxes from organic pools calculated as the quotient of the pool sizes to the corresponding

38 turnover times. Assuming that all pool sizes were in a steady state, the left side of the equations in Appendices A-C (Eqs. A1-

39 A5, B1-B6 and C1-C6) were all equal to zero. Adding the constraints in Appendix D (Eqs. D1-D11), we derived a system with

40 28 equations and 28 unknown variables (Table 1), so the estimates of the unknowns in GOLUM-CNP were all well constrained.

41 The unknown variables were solved by applying the 33 global spatially explicit observation-based estimates listed in Table 1

42 in these equations (Appendix E). The set of equations of the GOLUM-CNP model was solved for each 0.25 °×0.25 ° grid cell

1 using biome-mean N:C and P:C stoichiometric ratios, grid-cell specific values of C variables from Bloom et al. (2016) and the

2 gridded external N- and P-input and -output fields described above. In this computation, some processes are only solved by

3 mass balance and steady-state assumptions instead of explicitly calibrated. For example, we did not explicitly simulate various

4 pathways of N and P mineralization and immobilization. The N and P mineralization fluxes are computed as the product of

5 the decomposition of C in litter and SOM and their respective stoichiometries, and N and P immobilization fluxes are computed

6 by mass balance to match the higher N:C and P:C ratios in the SOM pool than the ratios in inputs to SOM from wood and

7 litter. Similar computations have been widely used in previous studies. For instance, N and P mineralization were computed

8 as the difference between nutrient demand of vegetation and the sum of external inputs and resorption in Cleveland et al. (2013,

9 Eqs. S5 and S6), assuming that the nutrients available to plants in soil do not change significantly at current stage. Such

10 computations based on mass balance and steady-state assumptions allow us to have a diagnostic modelling framework, but at

11 the same time capture observations of carbon fluxes, pools and pool stoichiometries.

12 　　　The inputs of the C cycle from original CARDAMOM dataset were provided as probability distributions, while other

13 datasets were provided only as mean values. In this study, we compute the GOLUM-CNP using the mean values of all the

14 input datasets to represent the mean behaviour of the C, N and P cycling.

15 　　　We present the C, N and P pools and the fluxes between them for each biome. We also aggregated the results at the global

16 scale and compared them with previous studies. We calculated some ecologically relevant quantities from the GOLUM-CNP

17 output. Following Cleveland et al. (2013), we defined the *openness* of N and P cycles as NO and PO that were calculated as

18 the percentage of the total plant uptake of nutrients (I_x, $X \in \{N,P\}$) from new nutrient inputs. Here, new nutrient inputs included

19 deposition (N_d) and biological fixation (N_{fix}) for N and deposition (P_d) and rock weathering (P_w) for P, and the total uptake of

20 nutrients by vegetation included the uptake from inorganic-N or -P pools (F_x, $X \in \{N,P\}$) and the resorbed nutrients (RSB_x,

21 $X \in \{N,P\}$), leading to:

22
$$XO = \frac{I_x}{F_x + RSB_x} \tag{1}$$

23 　　　The mean residence time of N and P for the entire ecosystem ($\tau_{X,eco}$, $X \in \{N,P\}$) was defined as the ratio of total modeled

24 pool mass (including plant, litter, SOM and inorganic pools) to all outgoing fluxes. The sum of all steady-state outgoing fluxes

25 equaled the sum of external input fluxes, so we calculated the mean residence time of N and P by:

26
$$\tau_{N,eco} = \frac{\sum_{i=1}^{5} N_i + N_{inorg}}{N_d + N_{fix}}$$
$$\tag{2}$$
$$\tau_{P,eco} = \frac{\sum_{i=1}^{5} P_i + P_{inorg}}{P_d + P_w}$$

27 　　　The *nutrient-use efficiencies* (NUE and PUE) were defined by:

28
$$XUE = \frac{GPP}{Fx} = \frac{NPP / f_{NPP}}{Fx} \tag{3}$$

29 where F_x ($X \in \{N,P\}$) is the annual uptake of inorganic soil N or P by plants, and f_{NPP} is the ratio of NPP to gross primary

30 production (GPP) from CARDAMOM. Our model used NPP as the input C flux for ecosystems, but we used GPP instead of

31 NPP in Eq. (3) to calculate XUE for comparing with the estimates based on *in situ* measurements by Gill and Finzi (2016),

32 which were also based on GPP. We thus used f_{NPP} only as an external variable in our modeling framework, and f_{NPP} was not

33 targeted when evaluating the sensitivities and uncertainties of the results (see below).

1   We tested the steady-state sensitivity (SS) of the model results to the observational data sets (inputs of the model listed

2   in Table 1) by linearizing the GOLUM-CNP model and its solver for calculating the first-order partial derivative of all outputs

3   relative to each input parameter:

4    $SS = \partial\mathbf{O}/\partial\mathbf{I}$ (4)

5   where $\mathbf{I}$ is the vector of the input variables, and $\mathbf{O}$ is the vector of the output variables. This approach directly provided a

6   sensitivity matrix, which allowed us to test the effect of the accuracy of the measurement of each input variable on the model

7   results for the N and P cycles. This method was similar to the "one-at-a-time" (OAT) approach used for sensitivity analysis in

8   previous C-N coupled modeling studies (Orwin et al., 2011; Shi et al., 2016; Zaehle and Friend, 2010) but did not require

9   running simulations by changing the inputs one at a time. This approach did not fully explore the possible range of values for

10   a given parameter, but provided comparable SS values for different parameters, which is useful when the full uncertainty

11   ranges of some parameters are unknown, e.g. uncertainty due to the inconsistent definitions between the measured pools in the

12   real world and the conceptual pools in the model, or the large uncertainty due to sparse observations for some biomes. The

13   input parameters had distinct magnitudes (and units), so we used the relative sensitivities, e.g. $SS = \partial\mathbf{O}/\mathbf{O}/(\partial\mathbf{I}/\mathbf{I})$, to compare

14   the sensitivities to different model inputs. For the sensitivity analysis, an SS of 1 indicates that a 1% increase (or decrease) in

15   a model input produces a 1% increase (or decrease) in the model output, and an SS of -0.5 indicates that a 1% increase (or

16   decrease) in the model input produces a -0.5% decrease (or increase) in the model output. The results of this sensitivity analysis

17   could be further used to investigate the sources of uncertainty in the outputs and to evaluate variances of the model outputs

18   using error propagation:

$$\boldsymbol{\varepsilon}_{\mathbf{O},i} = \frac{\partial\mathbf{O}}{\partial\mathbf{I}_i}\boldsymbol{\varepsilon}_{\mathbf{I},i}$$

19   $$\boldsymbol{\varepsilon}_{\mathbf{O}} = \sum_{i=1}^{n}\frac{\partial\mathbf{O}}{\partial\mathbf{I}_i}\boldsymbol{\varepsilon}_{\mathbf{I},i}$$ (5)

$$\Sigma_{\mathbf{O}} = E(\boldsymbol{\varepsilon}_{\mathbf{O}}{}^{\mathrm{T}}\boldsymbol{\varepsilon}_{\mathbf{O}})$$

20   where $\varepsilon_{\mathbf{I},i}$ is the error in the ith input data, $\varepsilon_{\mathbf{O},i}$ is the error propagated from the error in input i, $\varepsilon_{\mathbf{O}}$ is the error that accounts for

21   errors in all input data, E represents the expectation of a variable and $\Sigma_{\mathbf{O}}$ is the covariance matrix whose diagonal entries are

22   the variances of the outputs.

23   **3.3 Adjustments of CARDAMOM C cycle**

24   Biomass distributions in grassland-dominated biomes, including savannas, are skewed to low biomass, but has a high tail,

25   particularly in the dry tropics (Saatchi et al., 2011; Williams et al., 2013). We approximated the C-cycle state of the non-forest

26   biomes (TRG, TEG and TUN) by partitioning half of CARDAMOM woody NPP to foliar NPP and half to fine roots, in order

27   to better represent grassland C, N and P cycling across these biomes.

28   The CARDAMOM terrestrial C analysis did not assume steady states. Our goal, however, was to describe the steady

29   states of C, N and P cycling, because few global long-term observations associated with N and P were available to constrain

30   the model. We recalculated the C cycle based on a subset of the CARDAMOM results. Specifically, we used NPP and turnover

31   times of the C pools for 2001-2010 (Table 1) and recalculated the steady-state sizes of these pools and the transfers of C

32   between the pools represented in Fig. 1, solving Eqs. A1-A5 with their left sides as zeros. This steady-state transformation of

33   the CARDAMOM C cycle is assessed in Sect. 4.1.

Geoscientific
Model Development
Discussions

4 Results

4.1 Steady state C cycle

Table 2 shows the global C-pool sizes and main fluxes of the steady-state C cycle transformed from CARDAMOM, which are compared with the means and percentile ranges from the original non-steady-state CARDAMOM results. The differences between the steady-state transformed pool sizes and the original CARDAMOM results were within 10% for most C pools and fluxes. The largest differences were for the estimates of the foliar, fine-root and wood pools. The larger foliar and fine-root pools in the steady-state model were due to placing woody NPP into these two pools in the grassland grid cells. These pools, however, remained within the [5, 95th] percentile range of the original version. The pool size for global woody biomass was 37% smaller in the steady-state model (469 Pg) than the original CARDAMOM results but remained within its inter-quartile range (364-984 Pg). The largest difference in woody biomass in the steady-state model was for the northern temperate and boreal region (>35°N) (Fig. S1). Independent remote-sensing estimates for 30°N to 80°N were 4.76 ± 1.78 kg C m^{-2} for mean forest C density and 79.8 ± 29.9 Pg C for total forest C (Thurner et al., 2014), which were much lower than the original CARDAMOM values (9.55 kg C m^{-2} for mean forest C density across pixels defined as forest in Fig. 2, and 361 Pg C for total forest C) for this region. The forest woody biomass in the steady-state model for the C cycle for this region (6.51 kg C m^{-2} for mean forest C density and 181 Pg C for total forest C) was lower than that in the original CARDAMOM data set but still higher than that reported by Thurner et al. (2014). This inconsistency was largely due to the limited extent of the Thurner et al. (2014) map, which only covered ecosystems categorized as forests. Residual overestimation could also be due to the assumption of a steady state, and northern temperate and boreal forests may deviate substantially from their equilibrium for the current NPP (Pan et al., 2011), due to climate change and elevated CO_2. Furthermore, biomass removal by harvesting and from disturbance other than fires was not explicitly constrained in CARDAMOM, which also contributed to a high bias of the steady-state transformation of CARDAMOM. In the following sections, we used the steady-state CARDAMOM results in the GOLUM-CNP model, which was more appropriate for the interpretation of biome-scale C, N and P cycling, using the methodological steps outlined in Sect. 3.2 and 3.3.

4.2 Steady-state pool sizes and fluxes

Figure 3 summarizes the pool sizes and fluxes of N and P for the seven biomes (Fig. 3 a-g). The uptake fluxes of N and P were largest for tropical forests, mainly driven by the large NPP of this biome. Rates of N and P uptake were lower for temperate and boreal forests than tropical forests and for non-forest biomes than forests. The pool sizes of N and P in plants tended to decrease from tropical to boreal regions, mostly consistent with the C-pool sizes and their observed stoichiometries. Conversely, N and P contents in litter were larger for boreal forests, temperate grasslands and tundra ecosystems than the other biomes, mainly due to a longer turnover of the litter pool in these biomes. The N-pool size of SOM was also larger in boreal forests, temperate grasslands and tundra than the other biomes. The P-pool size in SOM, however, was smaller for boreal forests and tundra than the other biomes, consistent with the differences between the N:C and P:C ratios of boreal biomes compared to other biomes (Table S1). Inorganic-N and -P pools and leaching rates of N and P were higher in tropical forests, where runoff was higher than in the other biomes. Semi-arid tropical grassland (TRG) had high losses of N and P by fire and a low loss from leaching. The internal N and P fluxes within ecosystems were usually much larger than the external input fluxes and the output fluxes for all biomes, highlighting the dominant role of internal cycling of N and P, which differed from C cycles where NPP and losses by respiration were larger than any internal C flux.

The rate of total N input (deposition and fixation) aggregated to a global scale was 0.19 Pg N y^{-1} and equaled (by construction) the steady-state rate of total N loss. Total N uptake by plants was 0.68 Pg N y^{-1}. Our estimate of N denitrification was 0.10 Pg N y^{-1}, consistent with the independent estimate of global soil denitrification of 0.12 Pg N y^{-1} by Seitzinger et al. (2006) and within the range reported by other studies, from 0.04 Pg N y^{-1} (Houlton and Bai, 2009) to 0.29 Pg N y^{-1} (Galloway

1 et al., 2013). The global loss of N from leaching was 0.04 Pg N y^{-1}, also similar to the independent estimates by Galloway et

2 al. (2004, 2013) of 0.013-0.18 Pg N y^{-1} and by Houlton and Bai (2009) of 0.09 Pg N y^{-1}. The total input of P to the terrestrial

3 ecosystem was 0.007 Pg P y^{-1}, 86% from deposition (range from 71% for BOCF to 92% for TRG); only a small fraction was

4 from rock weathering (ranging from 8 to 29% across biomes). The loss of N by fire globally was 48 Tg N y^{-1} and accounted

5 for 26% of the total N loss. The loss of P by fire accounted for only 18% of the total P loss. Our estimate of the litter P mass

6 (0.03 Pg P) was similar to the estimate of 0.04 Pg P by the CABLE model (Wang et al. 2010) but was two-fold lower than the

7 estimate (0.08 Pg P) modeled by Goll et al. (2012). Our estimate of the P mass in plants (0.17 Pg P) was smaller than the

8 estimates modeled by Wang et al. (2010) (0.39 Pg P) and Goll et al. (2012) (0.23 Pg P).

9 **4.3 Implications for ecological research**

10 Figure 4 shows the latitudinal distribution of foliar N:P ratios in our model, a result directly from the distribution of the

11 seven biomes and C:N and C:P ratios. Foliar N:P ratios decreased on average from low to high latitudes. Estimates from

12 previous studies also followed this trend (Kerkhoff et al., 2005; McGroddy et al., 2004; Reich and Oleksyn, 2004) based on

13 foliar measurements. The mean N:P ratios in our study were in the middle of the range of observations for all latitudes. The

14 results of GOLUM-CNP better indicated the high N:P ratios between 20 ° to 40 °, where grassland is the dominant biome, than

15 the monotonic regressions (colored lines in Fig. 4) derived by Reich and Oleksyn (2004) and Kerkhoff et al. (2005) for foliar

16 data, implying that the use of stoichiometries at the scale of large biomes can identify the general features of the spatial

17 gradients of N and P cycling.

18 Figure 5a and 5b show the distribution of the openness for N and P in different ecosystems. New N in forest ecosystems

19 (due to deposition and biological fixation) accounted for 10% (BOCF) to 51% (TECF) of the total plant uptake of N, and new

20 P (due to deposition and rock weathering) accounted for only 3.5% (BOCF) to 15% (TRF) of the total plant uptake of P. The

21 openness of both N and P in grassland ecosystems decreased from the tropics to high latitudes. The residence times in

22 ecosystems were much longer for N and P than C (Table S2) and decreased from the tropics to boreal areas (Fig. 5c and 5d).

23 The openness and residence times of N and P together demonstrated the support of plant growth by external inputs and

24 internal cycling. For example, the residence time of N was longer in TECF than TRF, indicating lower rates of N fixation and

25 deposition in TECF than TRF. The openness of N, however, was higher in TECF than TRF, because the turnover times of

26 litter and SOM in TECF were almost twice those in TRF (Fig. 3), so a large amount of N was "locked" in litter and SOM in

27 TECF, and the net mineralization (gross mineralization minus gross immobilization) was much lower in TECF than TRF. The

28 importance of external N inputs was thus much larger in TECF than TRF. More N and P will be needed to support the additional

29 productivity in the future due to, for example, climate change or elevated CO_2 (Sun et al., 2017), so that areas with more

30 external inputs will more likely meet the additional nutrient demands. Meanwhile, consistently lower P than N openness in all

31 ecosystems suggested that plant growth may be ultimately constrained in the future by low P availability.

32 Figure 6 shows the diagnosed nutrient-use efficiencies from GOLUM-CNP outputs for the seven biomes. Tropical forest

33 had the lowest NUE, and its PUE was much higher than those of the other biomes (Fig. 6a), consistent with the general view

34 that P limits productivity more than N in tropical ecosystems (Gill and Finzi, 2016; Reich and Oleksyn, 2004). The values of

35 NUE and PUE were similar to each other for TEDF, TECF and BOCF. Nutrient-use efficiencies were about 3-fold lower for

36 non-forest biomes (Fig. 6b) than forest biomes, and both NUE and PUE decreased from tropical/C4 grassland to tundra.

37 **4.4 Sensitivity analysis**

38 Figure 7 shows the mean sensitivity of the nutrient-uptake fluxes (F_N and F_P), nutrient-use efficiencies (NUE and PUE),

39 pool sizes of inorganic N and P (N_{inorg} and P_{inorg}), N and P openness, residence times of N and P in the ecosystem ($\tau_{N,eco}$ and

40 $\tau_{P,eco}$) and residence times of N and P in plants ($\tau_{N,plant}$ and $\tau_{P,plant}$) to the input variables for the tropical-rainforest biome (TRF).

41 The sensitivities were similar for the other biomes (Figs. S2 and S3). The uptake of nutrients in GOLUM-CNP was determined

Geoscientific
Model Development
Discussions

1 by NPP, NPP-allocation fractions, observation-based nutrient:C ratios and resorption coefficients (Eqs E7 and E18), so N

2 uptake for tropical forest (Fig. 6a) was highly sensitive to NPP (1.0), NPP-allocation fractions (0.3) and the N:C ratio (0.4) of

3 the woody pool, and P uptake was sensitive to NPP (1.0) and foliar variables (0.5 for $\gamma_{C,1}$ and 0.5 for $\rho_{P,1}$; see Table 1 for the

4 definition of these variables). The nutrient-use efficiencies, defined in Eq. (1) as the ratio between GPP and the nutrient-uptake

5 fluxes (Eq. 3), were negatively sensitive to the input variables mentioned above. Estimates of the openness of N and P were

6 sensitive to input fluxes, NPP, NPP-allocation fractions and stoichiometric inputs. The turnover times of nutrients in whole

7 plants ($\tau_{N,plant}$ and $\tau_{P,plant}$) were sensitive to the input data in turnover times of the plant tissues ($\tau_{1,2,3}$), the allocation fractions

8 of NPP to different biomass pools ($\gamma_{1,2,3}$), the stoichiometry ($\rho_{X,1,2,3}$, $X \in \{N,P\}$) and the resorption coefficients ($\epsilon_{X,1}$, $X \in \{N,P\}$).

9 ## 5   Discussion

10   We developed a new observation-based modeling framework of global terrestrial N and P cycling built on a data-driven

11 C-cycle model and observed N:C and P:C stoichiometric ratios in different pools spatially averaged at the scale of large biomes

12 and observation-based estimates of the external input and output fluxes of N and P. This model was then used to estimate the

13 pool sizes and fluxes in N and P cycles and indicators of the coupling between nutrient and C cycling, including nutrient

14 openness, residence times in ecosystems and nutrient-use efficiencies. The data-driven estimates of steady-state global C, N

15 and P cycles are the first that are fully consistent with a large set of global observation-based data sets, under the condition of

16 current climate, deposition and CO_2 concentration.

17 ### 5.1 Sensitivity to C variables

18   Our estimates of nutrient-use efficiencies differed significantly from those estimated from *in situ* measurements (red

19 squares and diamonds in Fig. 4) by Gill and Finzi (2016), particularly the values of PUE for all biomes and NUE for temperate

20 and boreal forests. NUE and PUE are functions of the NPP-allocation fractions, stoichiometric ratios, resorption coefficients

21 and fractions of fire in the total outgoing C flux (Eqs 3 and E7, where NPP is canceled by the division). The CARDAMOM

22 observation-based analysis of the C cycle is the basis of the GOLUM-CNP modeling framework, so that errors and

23 uncertainties in CARDAMOM for the C cycle translate into errors and uncertainties of GOLUM-CNP. Quantitatively, the

24 sensitivity analysis (Figs. 7, S2 and S3) indicated that F_N and F_P, and thus NUE and PUE, were most sensitive to the NPP-

25 allocation fractions (especially to woody biomass) and foliar stoichiometry. We applied the sensitivity matrix (Eq. 5) to further

26 calculate the contribution of variances from each of these input variables, in which the uncertainties in the NPP-allocation and

27 fire fractions were obtained from CARDAMOM and the uncertainties (1-sigma) in the N:C and P:C stoichiometric ratios and

28 resorption coefficients were assumed to be 40%. This 40% uncertainty was larger than the uncertainty (20%) of the N:C ratios

29 used by Wang et al. (2010), so our estimate of the contribution of uncertainties from the stoichiometric ratios was relatively

30 large. The contribution of these different sources of uncertainty to the variances of NUE and PUE is shown in Fig. 8 for

31 temperate coniferous forests whose NUE and PUE deviated the most from the estimate by Gill and Finzi (2016). Fig. 8 shows

32 that the NPP-allocation fractions were the largest contributors to the total variances in NUE and PUE, which totaled >80%.

33   The NPP-allocation coefficients in CARDAMOM were only constrained indirectly by the satellite observations of LAI

34 and tropical aboveground biomass. The uncertainty of the CARDAMOM allocation fractions was thus substantial, especially

35 for non-tropical biomes where no biomass data were used (allocation-fraction $25^{th} – 75^{th}$ percentile ranges are typically >50%

36 of the mean). For example, the mean fraction of NPP allocated to woody biomass in CARDAMOM was >60% in most grids

37 (Fig. S4a), which is rare for field measurements (Chen et al., 2013; Doughty et al., 2015). The mean allocation of NPP to fine

38 roots may have been underestimated, characterized by too long a turnover time in CARDAMOM (range from <1 to 10 y)

39 compared to field measurements (<3 y for all ecosystems, Gill and Jackson, 2000; Green et al., 2005). The CARDAMOM

40 results indicated a turnover time of leaves in temperate and boreal biomes of <1 y, while Reich et al. (2014) indicated that the

Geoscientific
Model Development
Discussions

1   typical life span of conifer needles in evergreen coniferous forests depended on temperature and ranged from 2.5 to >10 y, this

2   inconsistency being attributed by Bloom et al. (2016) to the potential roles of seasonal MODIS LAI biases and to the presence

3   of understory vegetation across high-latitude ecosystems (Heiskanen et al., 2012).

4   Considering these inconsistencies between mean CARDAMOM values and *in situ* measurements, we conducted an

5   additional experiment in which the CARDAMOM fields were further adapted: 1) the mean NPP-allocation fractions to woody

6   biomass and the turnover time of woody biomass was divided by 1.5 to make sure that the NPP-allocation fractions to woody

7   biomass fall in the range of field measurements, 2) the foliage turnover time of TECF and BOCF forests and associated NPP-

8   allocation fractions were adjusted (keeping foliar biomass not changed) to match *in situ* observations (Reich et al., 2014) based

9   on the fitted relationship between the needle longevity and mean annual temperature from Reich et al. (2014), assuming that

10 understory vegetation plays a minimal role in C, N and P cycling and 3) Since in CARDAMOM, the NPP was constrained by

11 GPP (GPP being constrained by the observation of LAI and the relationship between LAI and GPP) and the observation of

12 biomass, additional adjustments were made to conserve the total NPP and pool sizes estimated from CARDAMOM by

13 allocating the residual NPP after the modifications from step 1 and 2 to fine roots, and adjusting the turnover time of fine roots

14 to conserve exactly the pool size of CARDAMOM (see Figs. S4-S7 for the adjusted variables and original CARDAMOM

15 values). With these adjustments, the new C cycle is more consistent with the reality, especially for variables that were not well

16 constrained in original CARDAMOM analysis. Fig. 9 shows the NUE and PUE from this new experiment based on this

17 modified version of the C cycle from CARDAMOM. The NUE and PUE were lower than those in Fig. 6 for the forest biomes,

18 especially for TECF and BOCF, which tended to decrease PUE from tropical to boreal forest. This distribution of PUE among

19 the biomes in Fig. 9 better matched the differences between biomes presented by Gill and Finzi (2016). The differences

20 between Fig. 9 and Fig. 6 illustrate how the results of the NUE and PUE are sensitive to the C variables and how the

21 uncertainties in the C cycle would be propagated to the estimates of N and P cycles. However, inconsistencies exist because

22 the methods used in this study and by Gill and Finzi (2016) are different. For example, Gill and Finzi (2016) notably used the

23 net mineralization rates of N and P to approximate plant uptake, because their differences were an order of magnitude smaller

24 than net nutrient mineralization. These authors used *in situ* measurements of net N mineralization but used a statistical model

25 to estimate P mineralization based on a soil-order-specific soil-P pool due to the lack of data (Yang and Post, 2011) and a

26 regression between soil-P turnover times and mean annual temperature. Their estimate of plant uptake was thus independent

27 of vegetation stoichiometry, which differed from our study. Gill and Finzi (2016) also used bootstrapping to sample the NPP

28 and net N (or P) mineralization from independent studies. Their estimates of NUE and PUE were thus not based on paired

29 data, so their estimates may contain some sampling errors.

5.2 Uncertainty of nutrient-cycle openness

31   The distribution of nutrient-cycle openness in the seven biomes was presented in Sect. 4.3 and Fig. 5. Our estimate of a

32 small openness of N and P in BOCF, and that the openness was smaller for the P than the N cycle, were consistent with the

33 estimates by Cleveland et al. (2013). Our estimates of the N openness, however, were about twice as large as the estimates of

34 Cleveland et al. (2013). This difference was due to the larger deposition fluxes in our study (globally 72 Tg N y^{-1}) than those

35 used by Cleveland et al. (2013) (33 Tg N y^{-1}; from Dentener, 2006), because Wang et al. (2017) used an atmospheric model

36 with higher horizontal resolution and an updated inventory of reactive-N (e.g. NO_x and NH_3) emission (Wang et al., 2017) and

37 also because Cleveland et al. (2013) also assumed that only 15% of deposited N was available to plants. Cleveland et al. (2013)

38 demonstrated that changing the fraction of biologically available deposited N to 100% did not significantly change the

39 openness, because N-deposition fluxes were generally smaller than N fixation and accounted for a small fraction of external

40 N inputs in their study. Our estimates of P openness were also larger than those by Cleveland et al. (2013), which was attributed

41 to the large differences in the estimates of P deposition between the two studies. Cleveland et al. (2013) used values of P

42 deposition reported by Mahowald et al. (2008), which were almost an order of magnitude lower than the estimates from Wang

Geoscientific
Model Development
Discussions

1   et al. (2017) that we used, arguably because of an underestimated contribution of anthropogenic P emissions and not accounting

2   for P in particles with diameters >10 µm (Wang et al., 2017). We also found that the P-cycle openness decreased from the

3   tropics to the boreal region, in contrast to the results by Cleveland et al. (2013). This also derives from the differences in the

4   spatial gradients of P deposition in the two studies. Mahowald et al. (2008) found that P deposition was largest in northern

5   Africa and that P deposition was within the same order of magnitude for tropical and temperate forests. Wang et al. (2017),

6   however, found that P deposition was much larger over tropical forests than other regions. The contrasting spatial gradients in

7   P deposition was likely due to the different models of atmospheric transport used by Wang et al. (2017) and Mahowald et al.

8   (2008). More importantly, most stations measuring total P deposition are in temperate regions, and measurements of P

9   deposition over tropical forests are very limited (Mahowald et al., 2008; Wang et al., 2017), so the estimates of P deposition

10   in the tropics were not well constrained by *in situ* observations and thus had large uncertainties. Differences in the spatial

11   gradients in nutrient-cycle openness between our study and the study by Cleveland et al. (2013) demonstrated the impact of

12   uncertain input data sets on the estimate of ecologically relevant quantities. The quantitative assessment of the uncertainties in

13   our estimates of openness, however, was difficult, because the potential uncertainties in these data sets were not systematically

14   evaluated within and between different estimates, and should therefore be addressed in future studies.

15   **5.3 Future research and data needs**

16   Our estimates of global N and P cycles were at the scale of large biomes. Recent studies of N and P cycles have relied on

17   biome-specific stoichiometry (Cleveland et al., 2013; Wang et al., 2010). Stoichiometry, however, is also highly variable

18   within biomes (Reich and Oleksyn, 2004). For example, Kattge et al. (2011) found that 40% of the variability in foliar N

19   content was within species (finer scale than that of large biomes) and suggested that these stoichiometric ratios may be better

20   represented by future trait-based estimates rather than fixed species-specific values. Some improvements have been made on

21   the variation of stoichiometric ratios across climatic and ecological gradients within and across biomes, and on the contribution

22   of plant traits and environmental conditions to these variations (Dong et al., 2017; Han et al., 2005; Meyerholt and Zaehle,

23   2015). However, it is still not sufficient to derive a globally gridded overview of the N and P cycles on current knowledge. A

24   better understanding of the stoichiometric variability and its drivers is still needed in terms of not only representing the large-

25   scale gradients but also reducing the uncertainties at local scale. New and spatially interpolated stoichiometric data sets should

26   partly overcome this problem, although uncertainties in the interpolation will need to be carefully propagated on GOLUM-

27   CNP outputs.

28   We assumed that all terrestrial ecosystems were at a steady state for 2001-2010 due to a lack of global constraints on the

29   dynamics of N and P cycling over a long period. Terrestrial ecosystems, however, are not currently at steady states (Luo, 2017;

30   Luo and Weng, 2011), due to climate change, increasing atmospheric CO_2 and anthropogenic disturbance (Friedlingstein et

31   al., 2006; Sitch et al., 2015). Zaehle (2013) reported that the terrestrial biosphere has accumulated 1.2 Pg N and 134.0 Pg C

32   since the pre-industrial period. Wang et al. (2017) also found that N and P deposition have changed dramatically over time.

33   The simulations by different models varies considerably, e.g. the responses of the biosphere to the increasing atmospheric CO_2

34   (Zaehle et al., 2014) and thus in future projections, because the current data sets have had little success in constraining all key

35   processes in most LSMs. Our results are a first step for evaluating global biogeochemical cycles. A transient simulation of N

36   and P cycling will be needed in future studies as more constraints on N and P cycles emerge to study the effects of climate

37   change, increasing CO_2 levels and disturbance on N and P cycles and their feedbacks.

38   The sensitivity matrix presented in Sect. 4.4 provides a useful tool for assessing the uncertainties in model outputs by

39   propagating the uncertainties in the model inputs. We applied this method to quantitatively assess the sources of uncertainties

40   in the estimated nutrient-use efficiencies (Sect. 5.1 and Fig. 8), but we also found that the uncertainties for some other quantities

41   were currently difficult to obtain, because the estimates of uncertainties were not available for all spatially explicit input data.

42   This sensitivity analysis can be used in future studies to quantify the contribution of each input data set to the uncertainty in

Geoscientific
Model Development
Discussions

1   other model outputs, to characterize the dominant sources of uncertainties in the estimated C, N and P processes and thus to

2   identify priorities for future data syntheses to fill the largest gaps in uncertainty. Future studies that provide global data sets

3   will need to include systematic evaluations and spatially explicit estimates of uncertainties in their data sets.

4   **6   Concluding remarks**

5   This study is a first attempt to combine observation-based estimates of C, N, P fluxes and pools in terrestrial ecosystems

6   into a consistent (steady-state) diagnostic model. Although there are considerable uncertainties in our results due to uncertain

7   and incomplete carbon cycle and nutrient observations, the main findings are: 1) external input of P from outside the ecosystem

8   contributes to a smaller plant P uptake than that of N, indicating a likely ultimate constraints of P on plant growth in the future,

9   2) tropical forests have the lowest N use efficiency and the largest P use efficiency, suggesting the adaptive response of this

10   biome to the low P availability in the tropics. The structure of GOLUM-CNP is analogous to most other process-based LSMs

11   describing carbon and nutrient interactions (e.g. Goll et al., 2012, 2017a; Medvigy et al., 2009; Parton et al., 2010; Thornton

12   et al., 2007; Wang et al., 2010; Weng and Luo, 2008; Xu-Ri and Prentice, 2008; Yang et al., 2009; Zaehle et al., 2014; Zaehle

13   and Friend, 2010), although these models have more processes and use complex equations to describe the dynamics controlling

14   carbon and nutrient distribution among pools and the turnover of each pool. The output of the GOLUM-CNP provides a

15   traceable tool, in which a consistency between different datasets of global C, N and P cycles has been achieved. Such a

16   framework can thus be used in the future to test the performance of these LSMs in the simulation of interactions between C,

17   N and P cycling.

18   **Code and data availability**

19   The source code and the map of the classification of seven large biomes are included in the Supplement. For the other

20   datasets that are listed in Table 1, it is encouraged to contact the first authors of the original references.

21   **Appendix A Equations for carbon cycle**

22   The carbon cycle framework is based on DALEC2 model (Bloom and Williams, 2015), except that we combined the

23   labile and foliage pools together since the labile pool in DALEC2 only transfer to foliage. There are five pools in the C cycle

24   (1: foliage; 2: fine roots; 3: wood; 4: litter; 5: SOM). The equations governing the change of C pools are given by:

25    $\frac{dC_1}{dt} = -\tau_1^{-1}C_1 + \gamma_1 Fc$ (A1)

26    $\frac{dC_2}{dt} = -\tau_2^{-1}C_2 + \gamma_2 Fc$ (A2)

27    $\frac{dC_3}{dt} = -\tau_3^{-1}C_3 + \gamma_3 Fc$ (A3)

28    $\frac{dC_4}{dt} = \tau_1^{-1}C_1\left(1 - f_{fireC,1}\right) + \tau_2^{-1}C_2\left(1 - f_{fireC,2}\right) - \tau_4^{-1}C_4$ (A4)

29    $\frac{dC_5}{dt} = \tau_3^{-1}C_3(1 - f_{fireC,3}) + \eta\tau_4^{-1}C_4 - \tau_5^{-1}C_5$ (A5)

30   The definitions of the symbols are listed in Table 1.

31   **Appendix B Equations for nitrogen cycle**

32   There are five organic N pools and one inorganic soil N pool. The N cycle are described by the following equations:

33    $\frac{dN_1}{dt} = -\tau_1^{-1}N_1(1 - \varepsilon_1) + \beta_1 Fn$ (B1)

34    $\frac{dN_2}{dt} = -\tau_2^{-1}N_2 + \beta_2 Fn$ (B2)

Geoscientific
Model Development
Discussions

1    $\frac{dN_3}{dt} = -\tau_3^{-1}N_3 + \beta_3 Fn$ (B3)

2    $\frac{dN_4}{dt} = \tau_1^{-1}N_1(1-\varepsilon_1)(1-f_{fireC,1}) + \tau_2^{-1}N_2(1-f_{fireC,2}) - \tau_4^{-1}N_4$ (B4)

3    $\frac{dN_5}{dt} = \tau_3^{-1}N_3(1-f_{fireC,3}) + \eta\tau_4^{-1}N_4 + N_{imob} - \tau_5^{-1}N_5$ (B5)

4    $\frac{dN_{inorg}}{dt} = \tau_5^{-1}N_5(1-f_{fireC,5}) + \tau_4^{-1}N_4(1-\eta-f_{fireC,4}) + N_d + N_{fix} - N_{imob} - f_{leach}N_{inorg} - f_{denit}N_{inorg} - Fn$

5   (B6)

6   The definitions of the symbols are listed in Table 1.

7   In Eq. B6, the fraction of inorganic N (f_{leach}) that is lost due to leaching is computed by soil water (Θ) and the sum of

8   drainage and surface runoff (q). We use the spatially explicit estimate of daily soil moisture derived from the European Centre

9   for Medium-Range Weather Forecasts (ECMWF) Interim Reanalysis (ERA-Interim/Land; Albergel et al., 2013; Balsamo et

10   al., 2015) (see Table 1), and the global gridded estimate of monthly mean runoff data from the Global Runoff Data Centre

11   (GRDC, http://www.grdc.sr.unh.edu/). Since the runoff data only have a monthly time step, we use the same value of runoff

12   for each day within one month. The leaching fraction at annual scale is thus computed by:

13    $f_{leach} = \sum_{d=1}^{365} \frac{q_i}{\Theta_i + q_i}$ (B7)

14   Of note is that in this computation, f_{leach} can exceed one, meaning that the turnover time of inorganic N pool is smaller

15   than one year (Wang et al., 2010).

Appendix C Equations for phosphorus cycle

17   There are five organic P pools and one inorganic soil P pool. The P cycle are described by the following equations:

18    $\frac{dP_1}{dt} = -\tau_1^{-1}P_1(1-\theta_1) + \varphi_1 Fp$ (C1)

19    $\frac{dP_2}{dt} = -\tau_2^{-1}P_2 + \varphi_2 Fp$ (C2)

20    $\frac{dP_3}{dt} = -\tau_3^{-1}P_3 + \varphi_3 Fp$ (C3)

21    $\frac{dP_4}{dt} = \tau_1^{-1}P_1(1-\theta_1)(1-f_{fireC,1}) + \tau_2^{-1}P_2(1-f_{fireC,2}) - \tau_4^{-1}P_4$ (C4)

22    $\frac{dP_5}{dt} = \tau_3^{-1}P_3(1-f_{fireC,3}) + \eta\tau_4^{-1}P_4 + P_{imob} - \tau_5^{-1}P_5$ (C5)

23    $\frac{dP_{inorg}}{dt} = \tau_5^{-1}P_5(1-f_{fireC,5}) + +\tau_4^{-1}P_4(1-\eta-f_{fireC,4}) + P_d + P_w + 0.75 Fire_P - P_{imob} - f_{leach}f_{dissolve}P_{inorg} -$

24    $f_{sorb}P_{inorg} + Fp$ (C6)

25   Where $Fire_P$ represent the P in the ecosystem that suffers from fire events:

26    $Fire_P = \tau_1^{-1}P_1(1-\theta_1)f_{fireC,1} + \tau_2^{-1}P_2 f_{fireC,2} + \tau_3^{-1}P_3 f_{fireC,3} + \tau_4^{-1}P_4 f_{fireC,4} + \tau_5^{-1}P_5 f_{fireC,5}$ (C7)

Appendix D Additional constraints

28   1) Under steady-state, the N:C and P:C ratios for the plants and soil are assumed to be constant, so that N_i and P_i can be

29   calculated by the production of the C pool size from CARDAMOM and the stoichiometry ratios for each pool from

30   Zechmeister-Boltenstern et al. (2015), except litter which has different definitions in CARDAMOM and Zechmeister-

31   Boltenstern et al. (2015):

32    $N_i = \rho_{N,i}C_i$ ($i = 1,2,3,5$)   (D1-D4)

33    $P_i = \rho_{P,i}C_i$ ($i = 1,2,3,5$)   (D5-D8)

34   2) The fraction of NPP, F_N and F_P allocations sum up to 1:

35    $\beta_1 + \beta_2 + \beta_3 = 1$ (D9)

1 $\varphi_1 + \varphi_2 + \varphi_3 = 1$ (D10)

2 3) The fraction of gaseous loss of N due to denitrification to the total inorganic N loss should satisfy the estimates by

3 using global δ^{15}N observations (f_{gasN}, Goll et al., 2017b):

4 $\dfrac{f_{denit}N_{inorg}}{f_{leach}N_{inorg} + f_{denit}N_{inorg}} = f_{gasN}$ (D11)

5 **7 Appendix E Solutions under steady-state assumption**

6 $C_i = F_c \gamma_{C,i} \tau_i \quad (i = 1,2,3)$ (E1-E4)

7 $C_4 = \left[\dfrac{C_1}{\tau_1}(1 - f_{fireC,1}) + \dfrac{C_2}{\tau_2}(1 - f_{fireC,2}) \right] \tau_4$ (E5)

8 $C_5 = \left[\dfrac{C_3}{\tau_3}(1 - f_{fireC,3}) + \dfrac{C_4}{\tau_4}(1 - f_{fireC,4}) \right] \tau_5$ (E6)

9 $F_N = F_c \left[\rho_{N,1}\gamma_{C,1}(1 - f_{fireC,1})(1 - \varepsilon_{N,1}) + \rho_{N,1}\gamma_{C,1}f_{fireC,1} + \rho_{N,2}\gamma_{C,2} + \rho_{N,2}\gamma_{C,3} \right]$ (E7)

10 $\gamma_{N,2} = \dfrac{\rho_{N,2}C_2}{\tau_2 F_N}$ (E8)

11 $\gamma_{N,3} = \dfrac{\rho_{N,3}C_3}{\tau_3 F_N}$ (E9)

12 $\gamma_{N,1} = 1 - \gamma_{N,2} - \gamma_{N,3}$ (E10)

13 $N_i = \rho_{N,i}C_i \quad (i = 1,2,3,5)$ (E11-E14)

14 $N_4 = \dfrac{\frac{\rho_{N,1}C_1}{\tau_1}(1 - f_{fireC,1}) + \frac{\rho_{N,2}C_2}{\tau_2}(1 - f_{fireC,2})}{\frac{C_1}{\tau_1}(1 - f_{fireC,1}) + \frac{C_2}{\tau_2}(1 - f_{fireC,2})} C_4$ (E15)

15 $N_{imorb} = \eta \left(\rho_{N,5} - \dfrac{N_4}{C_4} \right) \dfrac{C_4}{\tau_4} + \left(\rho_{N,5} - \dfrac{N_3}{C_3} \right) \dfrac{C_3}{\tau_3}(1 - f_{fireC,3})$ (E16)

16 $N_{inorg} = \dfrac{N_d + N_{fix} - \sum_{i=1}^{5} \left(\frac{N_i}{\tau_i} f_{fireC,i} \right)}{f_{leach}}$ (E17)

17 $F_P = F_c \left[\rho_{P,1}\gamma_{C,1}(1 - f_{fireC,1})(1 - \varepsilon_{P,1}) + \rho_{P,1}\gamma_{C,1}f_{fireC,1} + \rho_{P,2}\gamma_{C,2} + \rho_{P,2}\gamma_{C,3} \right]$ (E18)

18 $\gamma_{P,2} = \dfrac{\rho_{P,2}C_2}{\tau_2 F_P}$ (E19)

19 $\gamma_{P,3} = \dfrac{\rho_{P,3}C_3}{\tau_3 F_P}$ (E20)

20 $\gamma_{P,1} = 1 - \gamma_{P,2} - \gamma_{P,3}$ (E21)

21 $P_i = \rho_{P,i}C_i \quad (i = 1,2,3,5)$ (E22-E25)

22 $P_4 = \dfrac{\frac{\rho_{P,1}C_1}{\tau_1}(1 - f_{fireC,1}) + \frac{\rho_{P,2}C_2}{\tau_2}(1 - f_{fireC,2})}{\frac{C_1}{\tau_1}(1 - f_{fireC,1}) + \frac{C_2}{\tau_2}(1 - f_{fireC,2})} C_4$ (E26)

23 $P_{imorb} = \eta \left(\rho_{P,5} - \dfrac{P_4}{C_4} \right) \dfrac{C_4}{\tau_4} + \left(\rho_{P,5} - \dfrac{P_3}{C_3} \right) \dfrac{C_3}{\tau_3}(1 - f_{fireC,3})$ (E27)

24 $P_{inorg} = \dfrac{P_d + P_w - \sum_{i=1}^{5} \left(\frac{P_i}{\tau_i} f_{fireC,i} \right)}{f_{leach}f_{dissolve} + f_{sorb}}$ (E28)

Geoscientific
Model Development
Discussions

4   **References**

5   Albergel, C., Dorigo, W., Reichle, R. H., Balsamo, G., De Rosnay, P., Muñoz-Sabater, J., Isaksen, L., De Jeu, R. and Wagner,
6   W.: Skill and global trend analysis of soil moisture from reanalyses and microwave remote sensing, J. Hydrometeorol.,
7   14(4), 1259–1277, 2013.
8   Bai, E., Houlton, B. Z. and Wang, Y. P.: Isotopic identification of nitrogen hotspots across natural terrestrial ecosystems,
9   Biogeosciences, 9(8), 3287–3304, doi:10.5194/bg-9-3287-2012, 2012.
10   Balsamo, G., Albergel, C., Beljaars, A., Boussetta, S., Brun, E., Cloke, H., Dee, D., Dutra, E., Muñoz-Sabater, J., Pappenberger,
11   F. and others: ERA-Interim/Land: a global land surface reanalysis data set, Hydrol. Earth Syst. Sci., 19(1), 389–407,
12   2015.
13   Bloom, A. A. and Williams, M.: Constraining ecosystem carbon dynamics in a data-limited world: integrating ecological
14   "common sense" in a model–data fusion framework, Biogeosciences, 12(5), 1299–1315, 2015.
15   Bloom, A. A., Exbrayat, J.-F., Velde, I. R. van der, Feng, L. and Williams, M.: The decadal state of the terrestrial carbon cycle:
16   Global retrievals of terrestrial carbon allocation, pools, and residence times, Proc. Natl. Acad. Sci., 113(5), 1285–1290,
17   doi:10.1073/pnas.1515160113, 2016.
18   Bontemps, S., Defourny, P., Radoux, J., Van Bogaert, E., Lamarche, C., Achard, F., Mayaux, P., Boettcher, M., Brockmann,
19   C., Kirches, G. and others: Consistent global land cover maps for climate modelling communities: current achievements
20   of the ESA's land cover CCI, in Proceedings of the ESA Living Planet Symposium, Edimburgh, pp. 9–13. [online]
21   Available from: https://ftp.space.dtu.dk/pub/Ioana/papers/s274_2bont.pdf (Accessed 20 April 2017), 2013.
22   Bouwman, A. F., Lee, D. S., Asman, W. a. H., Dentener, F. J., Van Der Hoek, K. W. and Olivier, J. G. J.: A global high-
23   resolution emission inventory for ammonia, Glob. Biogeochem. Cycles, 11(4), 561–587, doi:10.1029/97GB02266, 1997.
24   Chen, G., Yang, Y. and Robinson, D.: Allocation of gross primary production in forest ecosystems: allometric constraints and
25   environmental responses, New Phytol., 200(4), 1176–1186, doi:10.1111/nph.12426, 2013.
26   Cleveland, C. C., Houlton, B. Z., Smith, W. K., Marklein, A. R., Reed, S. C., Parton, W., Grosso, S. J. D. and Running, S. W.:
27   Patterns of new versus recycled primary production in the terrestrial biosphere, Proc. Natl. Acad. Sci., 110(31), 12733–
28   12737, doi:10.1073/pnas.1302768110, 2013.
29   Dentener, F. J.: Global Maps of Atmospheric Nitrogen Deposition, 1860, 1993, and 2050, , doi:10.3334/ornldaac/830, 2006.
30   Dong, N., Prentice, I. C., Evans, B. J., Caddy-Retalic, S., Lowe, A. J. and Wright, I. J.: Leaf nitrogen from first principles:
31   field evidence for adaptive variation with climate, Biogeosciences, 14(2), 481–495, doi:10.5194/bg-14-481-2017, 2017.
32   Doughty, C. E., Metcalfe, D. B., Girardin, C. A. J., Amézquita, F. F., Cabrera, D. G., Huasco, W. H., Silva-Espejo, J. E.,
33   Araujo-Murakami, A., Da Costa, M. C., Rocha, W. and others: Drought impact on forest carbon dynamics and fluxes in
34   Amazonia, Nature, 519(7541), 78–82, 2015.
35   Elser, J. J., Bracken, M. E. S., Cleland, E. E., Gruner, D. S., Harpole, W. S., Hillebrand, H., Ngai, J. T., Seabloom, E. W.,
36   Shurin, J. B. and Smith, J. E.: Global analysis of nitrogen and phosphorus limitation of primary producers in freshwater,
37   marine and terrestrial ecosystems, Ecol. Lett., 10(12), 1135–1142, doi:10.1111/j.1461-0248.2007.01113.x, 2007.
38   Fekete, B. M., Vörösmarty, C. J. and Grabs, W.: High-resolution fields of global runoff combining observed river discharge
39   and simulated water balances, Glob. Biogeochem. Cycles, 16(3) [online] Available from:
40   http://onlinelibrary.wiley.com/doi/10.1029/1999GB001254/full (Accessed 8 May 2017), 2002.
41   Freney, J. R., Simpson, J. R. and Denmead, O. T.: Volatilization of ammonia, in Gaseous loss of nitrogen from plant-soil
42   systems, pp. 1–32, Springer. [online] Available from: http://link.springer.com/chapter/10.1007/978-94-017-1662-8_1
43   (Accessed 19 April 2017), 1983.
44   Friedlingstein, P., Cox, P., Betts, R., Bopp, L., Von Bloh, W., Brovkin, V., Cadule, P., Doney, S., Eby, M., Fung, I. and others:
45   Climate–carbon cycle feedback analysis: results from the C4MIP model intercomparison, J. Clim., 19(14), 3337–3353,
46   2006.
47   Galloway, J. N., Dentener, F. J., Capone, D. G., Boyer, E. W., Howarth, R. W., Seitzinger, S. P., Asner, G. P., Cleveland, C.
48   C., Green, P. A., Holland, E. A., Karl, D. M., Michaels, A. F., Porter, J. H., Townsend, A. R. and Vöosmarty, C. J.:
49   Nitrogen Cycles: Past, Present, and Future, Biogeochemistry, 70(2), 153–226, doi:10.1007/s10533-004-0370-0, 2004.
50   Galloway, J. N., Leach, A. M., Bleeker, A. and Erisman, J. W.: A chronology of human understanding of the nitrogen cycle,
51   Philos. Trans. R. Soc. B Biol. Sci., 368(1621), 20130120, doi:10.1098/rstb.2013.0120, 2013.
52   Gärdenäs, A. I., Ågren, G. I., Bird, J. A., Clarholm, M., Hallin, S., Ineson, P., Kätterer, T., Knicker, H., Nilsson, S. I., Näsholm,
53   T., Ogle, S., Paustian, K., Persson, T. and Stendahl, J.: Knowledge gaps in soil carbon and nitrogen interactions – From
54   molecular to global scale, Soil Biol. Biochem., 43(4), 702–717, doi:10.1016/j.soilbio.2010.04.006, 2011.
55   Giglio, L., Randerson, J. T. and Werf, G. R.: Analysis of daily, monthly, and annual burned area using the fourth-generation
56   global fire emissions database (GFED4), J. Geophys. Res. Biogeosciences, 118(1), 317–328, 2013.
57   Gill, A. L. and Finzi, A. C.: Belowground carbon flux links biogeochemical cycles and resource-use efficiency at the global
58   scale, Ecol. Lett., 19(12), 1419–1428, doi:10.1111/ele.12690, 2016.
59   Gill, R. A. and Jackson, R. B.: Global patterns of root turnover for terrestrial ecosystems, New Phytol., 147(1), 13–31,
60   doi:10.1046/j.1469-8137.2000.00681.x, 2000.

Geoscientific
Model Development
Discussions

1 Goll, D. S., Brovkin, V., Parida, B. R., Reick, C. H., Kattge, J., Reich, P. B., van Bodegom, P. M. and Niinemets, Ü.: Nutrient
2   limitation reduces land carbon uptake in simulations with a model of combined carbon, nitrogen and phosphorus cycling,
3   Biogeosciences, 9, 3547–3569, doi:10.5194/bg-9-3547-2012, 2012.
4 Goll, D. S., Vuichard, N., Maignan, F., Jornet-Puig, A., Sardans, J., Violette, A., Peng, S., Sun, Y., Kvakic, M., Guimberteau,
5   M., Guenet, B., Zaehle, S., Peñuelas, J., Janssens, I. and Ciais, P.: A representation of the phosphorus cycle for
6   ORCHIDEE (revision 3985), Geosci Model Dev Discuss, 2017, 1–39, doi:10.5194/gmd-2017-62, 2017a.
7 Goll, D. S., Winkler, A. J., Raddatz, T., Dong, N., Prentice, I. C., Ciais, P. and Brovkin, V.: Carbon-nitrogen interactions in
8   idealized simulations with JSBACH (version 3.10), Geosci Model Dev Discuss, 2017, 1–28, doi:10.5194/gmd-2016-304,
9   2017b.
10 Gordon, W. S. and Jackson, R. B.: Nutrient concentrations in fine roots, Ecology, 81(1), 275–280, 2000.
11 Green, J. J., Dawson, L. A., Proctor, J., Duff, E. I. and Elston, D. A.: Fine Root Dynamics in a Tropical Rain Forest is
12   Influenced by Rainfall, Plant Soil, 276(1–2), 23–32, doi:10.1007/s11104-004-0331-3, 2005.
13 Gruber, N. and Galloway, J. N.: An Earth-system perspective of the global nitrogen cycle, Nature, 451(7176), 293–296,
14   doi:10.1038/nature06592, 2008.
15 Han, W., Fang, J., Guo, D. and Zhang, Y.: Leaf nitrogen and phosphorus stoichiometry across 753 terrestrial plant species in
16   China, New Phytol., 168(2), 377–385, doi:10.1111/j.1469-8137.2005.01530.x, 2005.
17 Hartmann, J., Moosdorf, N., Lauerwald, R., Hinderer, M. and West, A. J.: Global chemical weathering and associated P-release
18   —   The   role   of   lithology,   temperature   and   soil   properties,   Chem.   Geol.,   363,   145–163,
19   doi:10.1016/j.chemgeo.2013.10.025, 2014.
20 Heiskanen, J., Rautiainen, M., Stenberg, P., Mõttus, M., Vesanto, V.-H., Korhonen, L. and Majasalmi, T.: Seasonal variation
21   in MODIS LAI for a boreal forest area in Finland, Remote Sens. Environ., 126, 104–115, 2012.
22 Hiederer, R. and Köchy, M.: Global soil organic carbon estimates and the harmonized world soil database, EUR, 79, 25225,
23   2011.
24 Houlton, B. Z. and Bai, E.: Imprint of denitrifying bacteria on the global terrestrial biosphere, Proc. Natl. Acad. Sci., 106(51),
25   21713–21716, doi:10.1073/pnas.0912111106, 2009.
26 Houlton, B. Z., Marklein, A. R. and Bai, E.: Representation of nitrogen in climate change forecasts, Nat. Clim. Change, 5(5),
27   398–401, doi:10.1038/nclimate2538, 2015.
28 Hungate, B. A., Dukes, J. S., Shaw, M. R., Luo, Y. and Field, C. B.: Nitrogen and Climate Change, Science, 302(5650), 1512–
29   1513, doi:10.1126/science.1091390, 2003.
30 Jahnke, R. A.: The phosphorus cycle, in Earth system science: From biogeochemical cycles to global change, pp. 360–376,
31   Elservier   Academic   Press,   San   Diego.   [online]   Available   from:
32   https://books.google.fr/books?hl=en&lr=&id=85YkdAm5tdoC&oi=fnd&pg=PA360&dq=The+Phosphorus+Cycle&ots
33   =ImiRpJyZLU&sig=ho0YXiy7pOAleQOCstOZc0iGtYs, 2000.
34 Kattge, J., Díaz, S., Lavorel, S., Prentice, I. C., Leadley, P., Bönisch, G., Garnier, E., Westoby, M., Reich, P. B., Wright, I. J.,
35   Cornelissen, J. H. C., Violle, C., Harrison, S. P., Van BODEGOM, P. M., Reichstein, M., Enquist, B. J., Soudzilovskaia,
36   N. A., Ackerly, D. D., Anand, M., Atkin, O., Bahn, M., Baker, T. R., Baldocchi, D., Bekker, R., Blanco, C. C., Blonder,
37   B., Bond, W. J., Bradstock, R., Bunker, D. E., Casanoves, F., Cavender-Bares, J., Chambers, J. Q., Chapin Iii, F. S.,
38   Chave, J., Coomes, D., Cornwell, W. K., Craine, J. M., Dobrin, B. H., Duarte, L., Durka, W., Elser, J., Esser, G., Estiarte,
39   M., Fagan, W. F., Fang, J., Fernández-Méndez, F., Fidelis, A., Finegan, B., Flores, O., Ford, H., Frank, D., Freschet, G.
40   T., Fyllas, N. M., Gallagher, R. V., Green, W. A., Gutierrez, A. G., Hickler, T., Higgins, S. I., Hodgson, J. G., Jalili, A.,
41   Jansen, S., Joly, C. A., Kerkhoff, A. J., Kirkup, D., Kitajima, K., Kleyer, M., Klotz, S., Knops, J. M. H., Kramer, K.,
42   Kühn, I., Kurokawa, H., Laughlin, D., Lee, T. D., Leishman, M., Lens, F., Lenz, T., Lewis, S. L., Lloyd, J., Llusià J.,
43   Louault, F., Ma, S., Mahecha, M. D., Manning, P., Massad, T., Medlyn, B. E., Messier, J., Moles, A. T., Müller, S. C.,
44   Nadrowski, K., Naeem, S., Niinemets, Ü., Nöllert, S., Nüske, A., Ogaya, R., Oleksyn, J., Onipchenko, V. G., Onoda, Y.,
45   Ordoñez, J., Overbeck, G., et al.: TRY – a global database of plant traits, Glob. Change Biol., 17(9), 2905–2935,
46   doi:10.1111/j.1365-2486.2011.02451.x, 2011.
47 Kerkhoff, A. J., Enquist, B. J., Elser, J. J. and Fagan, W. F.: Plant allometry, stoichiometry and the temperature-dependence
48   of primary productivity, Glob. Ecol. Biogeogr., 14(6), 585–598, doi:10.1111/j.1466-822X.2005.00187.x, 2005.
49 Klodd, A. E., Nippert, J. B., Ratajczak, Z., Waring, H. and Phoenix, G. K.: Tight coupling of leaf area index to canopy nitrogen
50   and phosphorus across heterogeneous tallgrass prairie communities, Oecologia, 182(3), 889–898, doi:10.1007/s00442-
51   016-3713-3, 2016.
52 Liu, Y., Wang, C., He, N., Wen, X., Gao, Y., Li, S., Niu, S., Butterbach-Bahl, K., Luo, Y. and Yu, G.: A global synthesis of
53   the rate and temperature sensitivity of soil nitrogen mineralization: latitudinal patterns and mechanisms, Glob. Change
54   Biol., 23(1), 455–464, doi:10.1111/gcb.13372, 2017.
55 Luo, Y.: The Third Dimension of Terrestrial Carbon Cycle Dynamics, 2017.
56 Luo, Y. and Weng, E.: Dynamic disequilibrium of the terrestrial carbon cycle under global change, Trends Ecol. Evol., 26(2),
57   96–104, 2011.
58 Mahowald, N., Jickells, T. D., Baker, A. R., Artaxo, P., Benitez-Nelson, C. R., Bergametti, G., Bond, T. C., Chen, Y., Cohen,
59   D. D., Herut, B., Kubilay, N., Losno, R., Luo, C., Maenhaut, W., McGee, K. A., Okin, G. S., Siefert, R. L. and Tsukuda,
60   S.: Global distribution of atmospheric phosphorus sources, concentrations and deposition rates, and anthropogenic
61   impacts, Glob. Biogeochem. Cycles, 22(4), GB4026, doi:10.1029/2008GB003240, 2008.
62 Manzoni, S., Trofymow, J. A., Jackson, R. B. and Porporato, A.: Stoichiometric controls on carbon, nitrogen, and phosphorus
63   dynamics in decomposing litter, Ecol. Monogr., 80(1), 89–106, 2010.
64 McGroddy, M. E., Daufresne, T. and Hedin, L. O.: Scaling of C:n:p Stoichiometry in Forests Worldwide: Implications of

Geoscientific
Model Development
Discussions

Open Access

1   Terrestrial Redfield-Type Ratios, Ecology, 85(9), 2390–2401, doi:10.1890/03-0351, 2004.
2   Medvigy, D., Wofsy, S. C., Munger, J. W., Hollinger, D. Y. and Moorcroft, P. R.: Mechanistic scaling of ecosystem function
3   and dynamics in space and time: Ecosystem Demography model version 2, J. Geophys. Res. Biogeosciences, 114(G1),
4   G01002, doi:10.1029/2008JG000812, 2009.
5   Melillo, J. M., Butler, S., Johnson, J., Mohan, J., Steudler, P., Lux, H., Burrows, E., Bowles, F., Smith, R., Scott, L. and others:
6   Soil warming, carbon–nitrogen interactions, and forest carbon budgets, Proc. Natl. Acad. Sci., 108(23), 9508–9512, 2011.
7   Meyerholt, J. and Zaehle, S.: The role of stoichiometric flexibility in modelling forest ecosystem responses to nitrogen
8   fertilization, New Phytol., 208(4), 1042–1055, doi:10.1111/nph.13547, 2015.
9   Myneni, R., Knyazikhin, Y. and Park, T.: MOD15A2H MODIS/Terra Leaf Area Index/FPAR 8-Day L4 Global 500m SIN
10   Grid V006, 2015.
11 Näsholm, T., Kielland, K. and Ganeteg, U.: Uptake of organic nitrogen by plants, New Phytol., 182(1), 31–48,
12   doi:10.1111/j.1469-8137.2008.02751.x, 2009.
13 Niemeyer, T., Niemeyer, M., Mohamed, A., Fottner, S. and Härdtle, W.: Impact of prescribed burning on the nutrient balance
14   of heathlands with particular reference to nitrogen and phosphorus, Appl. Veg. Sci., 8(2), 183–192, 2005.
15 Norby, R. J., Warren, J. M., Iversen, C. M., Medlyn, B. E. and McMurtrie, R. E.: CO_2 enhancement of forest productivity
16   constrained by limited nitrogen availability, Proc. Natl. Acad. Sci., 107(45), 19368–19373,
17   doi:10.1073/pnas.1006463107, 2010.
18 Orwin, K. H., Kirschbaum, M. U. F., St John, M. G. and Dickie, I. A.: Organic nutrient uptake by mycorrhizal fungi enhances
19   ecosystem carbon storage: a model-based assessment, Ecol. Lett., 14(5), 493–502, doi:10.1111/j.1461-
20   0248.2011.01611.x, 2011.
21 Pan, Y., Birdsey, R. A., Fang, J., Houghton, R., Kauppi, P. E., Kurz, W. A., Phillips, O. L., Shvidenko, A., Lewis, S. L.,
22   Canadell, J. G., Ciais, P., Jackson, R. B., Pacala, S. W., McGuire, A. D., Piao, S., Rautiainen, A., Sitch, S. and Hayes,
23   D.: A large and persistent carbon sink in the world's forests, Science, 333(6045), 988–93, doi:10.1126/science.1201609,
24   2011.
25 Parton, W. J., Hanson, P. J., Swanston, C., Torn, M., Trumbore, S. E., Riley, W. and Kelly, R.: ForCent model development
26   and testing using the Enriched Background Isotope Study experiment, J. Geophys. Res. Biogeosciences, 115(G4),
27   G04001, doi:10.1029/2009JG001193, 2010.
28 Peñuelas, J., Poulter, B., Sardans, J., Ciais, P., Velde, M. van der, Bopp, L., Boucher, O., Godderis, Y., Hinsinger, P., Llusia,
29   J., Nardin, E., Vicca, S., Obersteiner, M. and Janssens, I. A.: Human-induced nitrogen–phosphorus imbalances alter
30   natural and managed ecosystems across the globe, Nat. Commun., 4, ncomms3934, doi:10.1038/ncomms3934, 2013.
31 Poulter, B., MacBean, N., Hartley, A., Khlystova, I., Arino, O., Betts, R., Bontemps, S., Boettcher, M., Brockmann, C.,
32   Defourny, P., Hagemann, S., Herold, M., Kirches, G., Lamarche, C., Lederer, D., Ottlé, C., Peters, M. and Peylin, P.:
33   Plant functional type classification for earth system models: results from the European Space Agency's Land Cover
34   Climate Change Initiative, Geosci Model Dev, 8(7), 2315–2328, doi:10.5194/gmd-8-2315-2015, 2015.
35 Qian, Y., Miao, S. L., Gu, B. and Li, Y. C.: Estimation of postfire nutrient loss in the Florida Everglades, J. Environ. Qual.,
36   38(5), 1812–1820, 2009.
37 Reich, P. B. and Oleksyn, J.: Global patterns of plant leaf N and P in relation to temperature and latitude, Proc. Natl. Acad.
38   Sci. U. S. A., 101(30), 11001–11006, 2004.
39 Reich, P. B., Oleksyn, J., Wright, I. J., Niklas, K. J., Hedin, L. and Elser, J. J.: Evidence of a general 2/3-power law of scaling
40   leaf nitrogen to phosphorus among major plant groups and biomes, Proc. R. Soc. Lond. B Biol. Sci., 277(1683), 877–
41   883, doi:10.1098/rspb.2009.1818, 2010.
42 Reich, P. B., Rich, R. L., Lu, X., Wang, Y.-P. and Oleksyn, J.: Biogeographic variation in evergreen conifer needle longevity
43   and impacts on boreal forest carbon cycle projections, Proc. Natl. Acad. Sci., 111(38), 13703–13708, 2014.
44 Saatchi, S. S., Harris, N. L., Brown, S., Lefsky, M., Mitchard, E. T., Salas, W., Zutta, B. R., Buermann, W., Lewis, S. L.,
45   Hagen, S. and others: Benchmark map of forest carbon stocks in tropical regions across three continents, Proc. Natl. Acad.
46   Sci., 108(24), 9899–9904, 2011.
47 Schimel, J. P. and Bennett, J.: Nitrogen mineralization: challenges of a changing paradigm, Ecology, 85(3), 591–602, 2004.
48 Schimel, J. P. and Chapin, F. S.: Tundra Plant Uptake of Amino Acid and NH4+ Nitrogen in Situ: Plants Complete Well for
49   Amino Acid N, Ecology, 77(7), 2142–2147, doi:10.2307/2265708, 1996.
50 Seitzinger, S., Harrison, J. A., Böhlke, J. K., Bouwman, A. F., Lowrance, R., Peterson, B., Tobias, C. and Drecht, G. V.:
51   Denitrification across landscapes and waterscapes: a synthesis, Ecol. Appl., 16(6), 2064–2090, 2006.
52 Shi, Z., Yang, Y., Zhou, X., Weng, E., Finzi, A. C. and Luo, Y.: Inverse analysis of coupled carbon–nitrogen cycles against
53   multiple datasets at ambient and elevated CO_2, J. Plant Ecol., 9(3), 285–295, 2016.
54 Sitch, S., Friedlingstein, P., Gruber, N., Jones, S. D., Murray-Tortarolo, G., Ahlström, A., Doney, S. C., Graven, H., Heinze,
55   C., Huntingford, C. and others: Recent trends and drivers of regional sources and sinks of carbon dioxide, Biogeosciences,
56   12(3), 653–679, 2015.
57 Sun, Y., Peng, S., Goll, D. S., Ciais, P., Guenet, B., Guimberteau, M., Hinsinger, P., Janssens, I. A., Peñuelas, J., Piao, S.,
58   Poulter, B., Violette, A., Yang, X., Yin, Y. and Zeng, H.: Diagnosing phosphorus limitations in natural terrestrial
59   ecosystems in carbon cycle models, Earths Future, 5(7), 730–749, doi:10.1002/2016EF000472, 2017.
60 Sutton, M. A., Simpson, D., Levy, P. E., Smith, R. I., Reis, S., Van Oijen, M. and De Vries, W. I. M.: Uncertainties in the
61   relationship between atmospheric nitrogen deposition and forest carbon sequestration, Glob. Change Biol., 14(9), 2057–
62   2063, 2008.
63 Thornton, P. E., Lamarque, J.-F., Rosenbloom, N. A. and Mahowald, N. M.: Influence of carbon-nitrogen cycle coupling on
64   land model response to CO_2 fertilization and climate variability, Glob. Biogeochem. Cycles, 21(4), GB4018,

1   doi:10.1029/2006GB002868, 2007.

2 Thurner, M., Beer, C., Santoro, M., Carvalhais, N., Wutzler, T., Schepaschenko, D., Shvidenko, A., Kompter, E., Ahrens, B.,
3   Levick, S. R. and Schmullius, C.: Carbon stock and density of northern boreal and temperate forests, Glob. Ecol.
4   Biogeogr., 23(3), 297–310, doi:10.1111/geb.12125, 2014.

5 Ver, L. M. B., Mackenzie, F. T. and Lerman, A.: Biogeochemical responses of the carbon cycle to natural and human
6   perturbations; past, present, and future, Am. J. Sci., 299(7–9), 762–801, 1999.

7 Vitousek, P. M. and Howarth, R. W.: Nitrogen limitation on land and in the sea: how can it occur?, Biogeochemistry, 13(2),
8   87–115, 1991.

9 Wang, R., Goll, D., Balkanski, Y., Hauglustaine, D., Boucher, O., Ciais, P., Janssens, I., Penuelas, J., Guenet, B., Sardans, J.
10   and others: Global forest carbon uptake due to nitrogen and phosphorus deposition from 1850 to 2100, Glob. Change
11   Biol. [online] Available from: http://onlinelibrary.wiley.com/doi/10.1111/gcb.13766/full, 2017.

12 Wang, S., Grant, R. F., Verseghy, D. L. and Black, T. A.: Modelling plant carbon and nitrogen dynamics of a boreal aspen
13   forest in CLASS — the Canadian Land Surface Scheme, Ecol. Model., 142(1–2), 135–154, doi:10.1016/S0304-
14   3800(01)00284-8, 2001.

15 Wang, Y. P., Law, R. M. and Pak, B.: A global model of carbon, nitrogen and phosphorus cycles for the terrestrial biosphere,
16   Biogeosciences, 7(7) [online] Available from:
17   http://search.proquest.com/docview/757608124/abstract/B62E84E06C7F4CC7PQ/1 (Accessed 7 March 2017), 2010.

18 Wang, Y.-P. and Houlton, B. Z.: Nitrogen constraints on terrestrial carbon uptake: Implications for the global carbon-climate
19   feedback, Geophys. Res. Lett., 36(24), L24403, doi:10.1029/2009GL041009, 2009.

20 Weng, E. and Luo, Y.: Soil hydrological properties regulate grassland ecosystem responses to multifactor global change: A
21   modeling analysis, J. Geophys. Res. Biogeosciences, 113(G3) [online] Available from:
22   http://onlinelibrary.wiley.com/doi/10.1029/2007JG000539/full, 2008.

23 Wieder, W. R., Cleveland, C. C., Smith, W. K. and Todd-Brown, K.: Future productivity and carbon storage limited by
24   terrestrial nutrient availability, Nat. Geosci., 8(6), 441, 2015.

25 Williams, M., Schwarz, P. A., Law, B. E., Irvine, J. and Kurpius, M. R.: An improved analysis of forest carbon dynamics using
26   data assimilation, Glob. Change Biol., 11(1), 89–105, 2005.

27 Williams, M., Hill, T. C. and Ryan, C. M.: Using biomass distributions to determine probability and intensity of tropical forest
28   disturbance, Plant Ecol. Divers., 6(1), 87–99, doi:10.1080/17550874.2012.692404, 2013.

29 Xu-Ri and Prentice, I. C.: Terrestrial nitrogen cycle simulation with a dynamic global vegetation model, Glob. Change Biol.,
30   14(8), 1745–1764, doi:10.1111/j.1365-2486.2008.01625.x, 2008.

31 Yang, X. and Post, W. M.: Phosphorus transformations as a function of pedogenesis: A synthesis of soil phosphorus data using
32   Hedley fractionation method, Biogeosciences, 8(10) [online] Available from:
33   http://search.proquest.com/docview/1012313736/abstract/28DB515C4ABC499BPQ/1 (Accessed 7 March 2017), 2011.

34 Yang, X., Wittig, V., Jain, A. K. and Post, W.: Integration of nitrogen cycle dynamics into the Integrated Science Assessment
35   Model for the study of terrestrial ecosystem responses to global change, Glob. Biogeochem. Cycles, 23(4) [online]
36   Available from: http://onlinelibrary.wiley.com/doi/10.1029/2009GB003474/full (Accessed 6 April 2017), 2009.

37 Yang, X., Post, W. M., Thornton, P. E. and Jain, A.: The distribution of soil phosphorus for global biogeochemical modeling,
38   Biogeosciences, 10(4), 2525, 2013.

39 Yang, X., Thornton, P. E., Ricciuto, D. M. and Post, W. M.: The role of phosphorus dynamics in tropical forests – a modeling
40   study using CLM-CNP, Biogeosciences, 11(6), 1667–1681, doi:10.5194/bg-11-1667-2014, 2014.

41 Zaehle, S.: Terrestrial nitrogen–carbon cycle interactions at the global scale, Philos. Trans. R. Soc. Lond. B Biol. Sci.,
42   368(1621), 20130125, doi:10.1098/rstb.2013.0125, 2013.

43 Zaehle, S. and Dalmonech, D.: Carbon–nitrogen interactions on land at global scales: current understanding in modelling
44   climate biosphere feedbacks, Curr. Opin. Environ. Sustain., 3(5), 311–320, doi:10.1016/j.cosust.2011.08.008, 2011.

45 Zaehle, S. and Friend, A. D.: Carbon and nitrogen cycle dynamics in the O-CN land surface model: 1. Model description, site-
46   scale evaluation, and sensitivity to parameter estimates, Glob. Biogeochem. Cycles, 24(1), GB1005,
47   doi:10.1029/2009GB003521, 2010.

48 Zaehle, S., Medlyn, B. E., De Kauwe, M. G., Walker, A. P., Dietze, M. C., Hickler, T., Luo, Y., Wang, Y.-P., El-Masri, B.,
49   Thornton, P., Jain, A., Wang, S., Warlind, D., Weng, E., Parton, W., Iversen, C. M., Gallet-Budynek, A., McCarthy, H.,
50   Finzi, A., Hanson, P. J., Prentice, I. C., Oren, R. and Norby, R. J.: Evaluation of 11 terrestrial carbon–nitrogen cycle
51   models against observations from two temperate Free-Air CO2 Enrichment studies, New Phytol., 202(3), 803–822,
52   doi:10.1111/nph.12697, 2014.

53 Zaehle, S., Jones, C. D., Houlton, B., Lamarque, J.-F. and Robertson, E.: Nitrogen availability reduces CMIP5 projections of
54   twenty-first-century land carbon uptake, J. Clim., 28(6), 2494–2511, 2015.

55 Zechmeister-Boltenstern, S., Keiblinger, K. M., Mooshammer, M., Peñuelas, J., Richter, A., Sardans, J. and Wanek, W.: The
56   application of ecological stoichiometry to plant–microbial–soil organic matter transformations, Ecol. Monogr., 85(2),
57   133–155, 2015.

58 Zhang, Q., Wang, Y. P., Pitman, A. J. and Dai, Y. J.: Limitations of nitrogen and phosphorous on the terrestrial carbon uptake
59   in the 20th century, Geophys. Res. Lett., 38(22), L22701, doi:10.1029/2011GL049244, 2011.

60 Zhu, Q. and Zhuang, Q.: Modeling the effects of organic nitrogen uptake by plants on the carbon cycling of boreal forest and
61   tundra ecosystems, Biogeosciences, 10(12), 7943–7955, 2013.

62

1   **Table 1** Global spatially explicit observation-based estimates of model variables used as input data sets and the unknowns
2   estimated in this study (including the symbols for each variable/parameter).

Variable	Definition	Description	References
Inputs: carbon cycle			
F_c	NPP	Spatially resolved model-data fusion estimates	CARDAMOM; Bloom et al., 2016
$\tau_{i=1,2,3,4,5}$	Residence time of foliage, fine roots, wood, litter and SOM	Spatially resolved model-data fusion estimates	CARDAMOM; Bloom et al., 2016
$\gamma_{C,\ i=1,2,3}$	Fraction of NPP allocated to foliage, fine roots and wood	Spatially resolved model-data fusion estimates	CARDAMOM; Bloom et al., 2016
$f_{fireC,\ i=1,2,3,4,5}$	Fraction of fire to total outgoing flux from foliage, fine roots, wood, litter and SOM	Spatially resolved model-data fusion estimates	CARDAMOM; Bloom et al., 2016
η	Fraction of litter outflux that enters SOM	Spatially resolved model-data fusion estimates	
Inputs: nitrogen cycle			
$\rho_{N,\ i=1,2,3,5}$	N:C ratio in foliage, fine roots, wood and SOM	Biome-scale synthesis based on *in situ* measurements	Zechmeister-Boltenstern et al., 2015
f_{leach}	Fraction of inorganic N (or P) lost due to leaching (Eq. B7)	Spatially resolved reanalysis by model; Model result, scaled to match measurements	Balsamo et al., 2015 Fekete et al., 2002
$\varepsilon_{N,\ 1}$	Resorption coefficient of N in foliage	Biome-scale synthesis based on *in situ* measurements	Zechmeister-Boltenstern et al., 2015
N_d	N deposition	Spatially resolved model result, scaled to match *in situ* measurements	Wang et al., 2017
N_{fix}	N fixation	Spatially resolved model result, scaled to match the estimates of NPP and N:C ratios	Peng et al., submitted
f_{gas}	Fraction of denitrification to the total loss of inorganic N	Spatially resolved process-based statistical model result	Goll et al., 2017b
Inputs: phosphorus cycle			
$\rho_{P,\ i=1,2,3,5}$	P:C ratio in foliage, fine roots, wood and SOM	Biome-scale synthesis based on *in situ* measurements	Zechmeister-Boltenstern et al., 2015
$f_{dissolved}$	Fraction of inorganic P that is dissolved in the soil water	*In situ* measurements, averaged based on soil order	Yang and Post, 2011
f_{sorb}	Fraction of inorganic P that is transformed to strongly sorbed P	Assumed constant	Goll et al., 2017a
$\varepsilon_{P,\ 1}$	Resorption coefficient of P in foliage	Biome-scale synthesis based on *in situ* measurements	Zechmeister-Boltenstern et al., 2015
P_d	P deposition	Spatially resolved model result, scaled to match *in situ* measurements	Wang et al., 2017
P_d	P weathering	Spatially resolved model result, scaled to match observed data	Hartmann et al., 2014
Unknowns estimated from mass balance assuming steady state			
$C_{i=1,2,3,4,5}$	C pool of foliage, fine roots, wood, litter and SOM	Pools	
F_N	N uptake from inorganic-N pool by vegetation	Flux	
$\gamma_{N,\ i=1,2,3}$	Fraction of F_N allocated to foliage, fine roots and wood	Allocation fractions	
$N_{i=1,2,3,4,5}$	N in foliage, fine roots, wood, litter and SOM	Pools	
N_{imob}	N immobilization flux	Pools	
f_{denit}	Annual denitrification rate	Rate	
N_{inorg}	Inorganic-N pool	Pool	
F_P	P uptake from inorganic-P pool by vegetation	Flux	
$\gamma_{P,\ i=1,2,3}$	Fraction of Fp allocated to foliage, fine roots and wood	Allocation fractions	
$P_{i=1,2,3,4,5}$	P in foliage, fine roots, wood, litter and SOM	Pools	
P_{imob}	P immobilization flux	Flux	
P_{inorg}	Inorganic-P pool	Pool	

3

4

Geoscientific
Model Development
Discussions

1   **Table 2** Global annual mean C-pool sizes, NPP and heterotrophic-respiration fluxes in the C-cycle model assuming steady
2   states, compared to the means and percentile ranges from the original CARDAMOM results.

	This study	Original CARDAMOM				
		5th percentile	25th percentile	Mean	75th percentile	95th percentile
Foliage-pool size (Pg C)	23	3.2	7	15	21	34
Fine-root-pool size (Pg C)	27	1.9	5	18	25	56
Wood-pool size (Pg C)	493	193	364	755	984	1850
Litter-pool size (Pg C)	20	1.3	4	22	26	88
SOM-pool size (Pg C)	1421	749	1100	1557	1882	2771
NPP (Pg C y^{-1})	52.5	Not given	39	52	63	Not given
Fire (Pg C y^{-1})	1.5	Not given	1.3	1.7	2.0	Not given
Heterotrophic respiration (Pg C y^{-1})	51	Not given	37	54	67	Not given

3

4
5
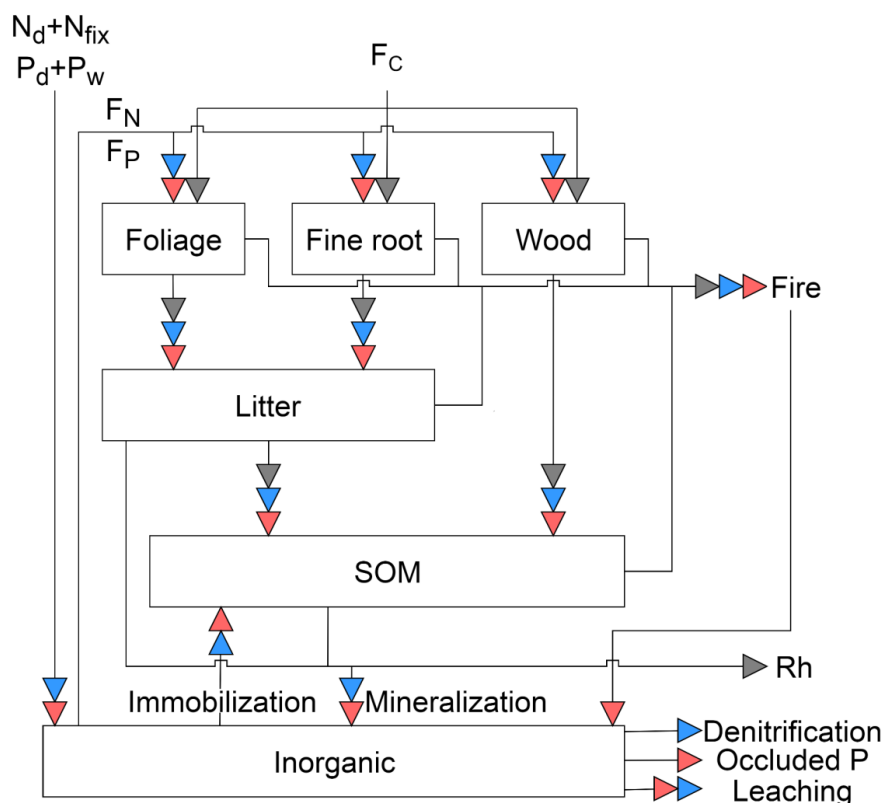
Figure 1 Schematic representation of the pools and fluxes in the C, N and P cycles within GOLUM-CNP. The gray, blue and red arrows represent C, N and P fluxes, respectively. Plants are divided into foliar, fine root and wood pools, where the wood pool includes woody stems and coarse roots. Litter and soil are two separate pools. The inorganic pool represents the nutrient sources in the soil that are available for plant uptake. Arrows between the pools represent the directions of C, N and P flow between pools. External inputs of N and P are atmospheric deposition (N_d and P_d), biological N fixation (N_{fix}) and P released by rock weathering (P_w). External losses of N occur by fire, leaching and denitrification. External losses of P occur by fire, leaching and transfer to occluded P in the soil. F_C is net primary production (NPP) and Rh is heterotrophic respiration. F_N and F_P are the plant uptake of N and P from the inorganic pool, respectively. Mineralization of N and P is modeled along with litter and SOM decomposition, and N and P immobilization is modeled by a flux from the inorganic pool to SOM.

1
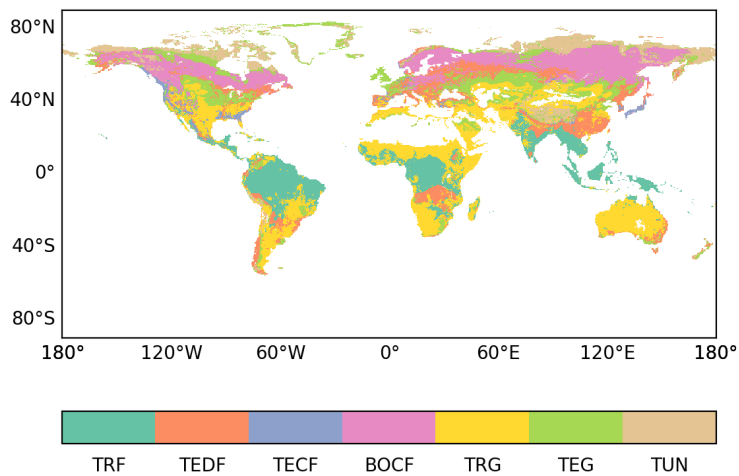
Figure 2 ESA CCI land-cover map classified into the seven large biomes for which average N:C and P:C ratios for each carbon
pool are available, at 0.25 °×0.25 ° resolution: tropical rainforests (TRF), temperate deciduous forests (TEDF), temperate
coniferous forests (TECF), boreal coniferous forests (BOCF), tropical/C4 grasslands (TRG), temperate/C3 grasslands (TEG)
and tundra (TUN).

6

Geoscientific
Model Development
Discussions
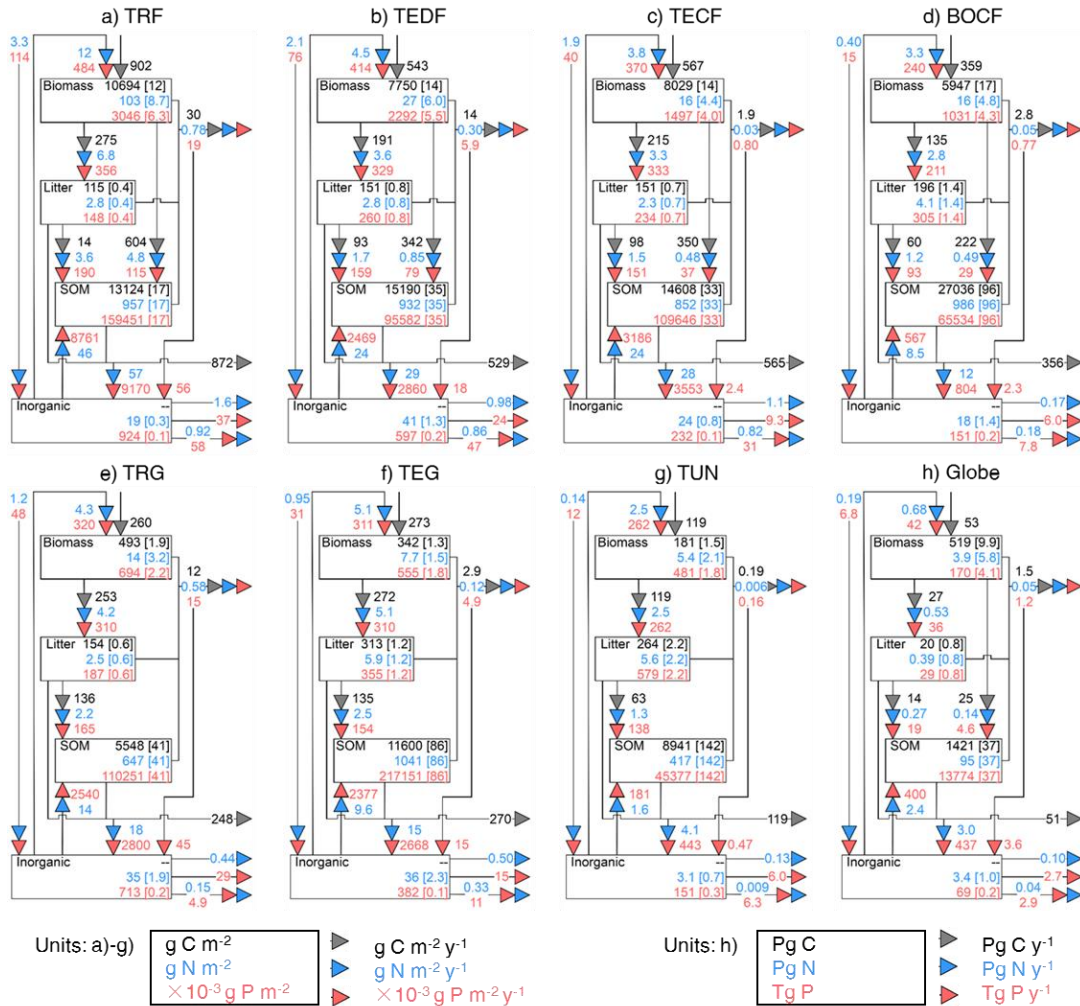
Figure 3 Fluxes (numbers along arrows), mean residence times (in parentheses) and pool sizes of the N (blue) and P (red) cycles in the terrestrial biosphere at steady state for the large biomes (a-g) and globe (h). The targeted biomes are tropical rainforests (TRF, a), temperate deciduous forests (TEDF, b), temperate coniferous forests (TECF, c), boreal coniferous forests (BOCF, d), tropical/C4 grasslands (TRG, e), temperate/C3 grasslands (TEG, f) and tundra (TUN, g).

1
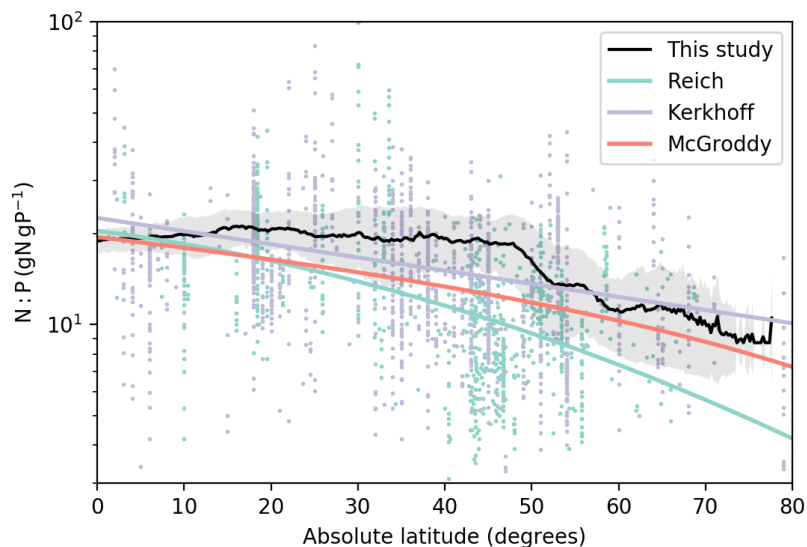
Figure 4 Relationship between foliar N:P ratios (gN gP^{-1}) and absolute latitude. The black line is the mean N:P ratios from
this study, and the shaded area is the one-sigma standard deviation of the N:P ratios for specific latitude. Colored lines are the
regression trends of foliar N:P ratios as a function of absolute latitude from Reich and Oleksyn (2004; green), Kerkhoff et al.
(2005; blue) and McGroddy et al. (2004; red). Dots are the raw data that Reich and Oleksyn (2004; green) and Kerkhoff et al.
(2005; blue) used to derive their regression trends.
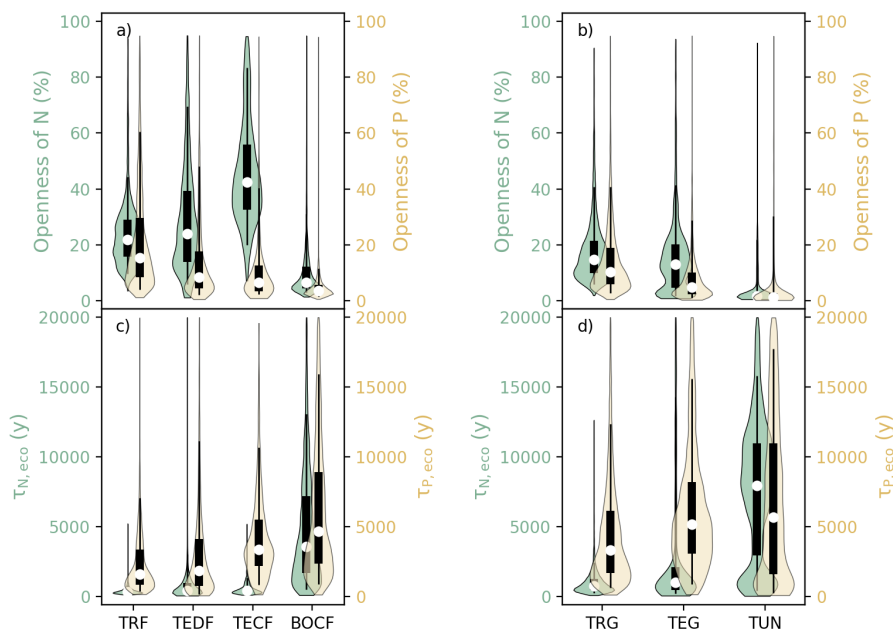
Figure 5 Violin plots of the openness of N and P cycling (the percentage of total plant uptake of N and P attributed to new nutrient inputs) for a) forest and b) grassland biomes. Residence times of N ($\tau_{N,eco}$) and P ($\tau_{P,eco}$) in c) forest ecosystems and d) grassland biomes. Open circles are medians of all grid cells within each biome, with balloons representing the probability density distribution of each value. Black whiskers indicate interquartile (thick) and 95% confidence intervals (thin). The biomes are tropical rainforests (TRF), temperate deciduous forests (TEDF), temperate coniferous forests (TECF), boreal coniferous forests (BOCF), tropical/C4 grasslands (TRG), temperate/C3 grasslands (TEG) and tundra (TUN).
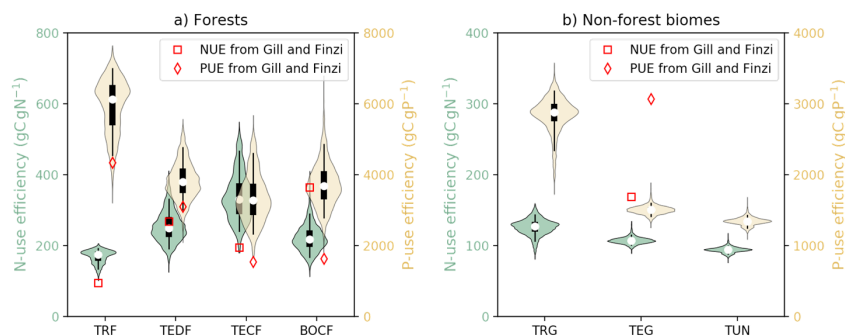
Figure 6 Violin plots of N- and P-use efficiencies (NUE and PUE, the nutrient uptake by plants divided by GPP) of seven biomes. Open circles are medians of all grid cells within each biome, with balloons representing the probability density distribution of each value. Black whiskers indicate interquartile (thick) and 95% confidence intervals (thin). a) Forest biomes, including tropical rainforests (TRF), temperate deciduous (TEDF), temperate coniferous (TECF) and boreal coniferous forests (BOCF). b) Grassland biomes, including tropical/C4 (TRG), temperate/C3 grasslands (TEG) and tundra (TUN). Red squares (NUE) and diamonds (PUE) are the independent estimates from site observations and other generic data sets compiled and harmonized by Gill and Finzi (2016) based on site measurements of GPP and net N/P mineralization.

1
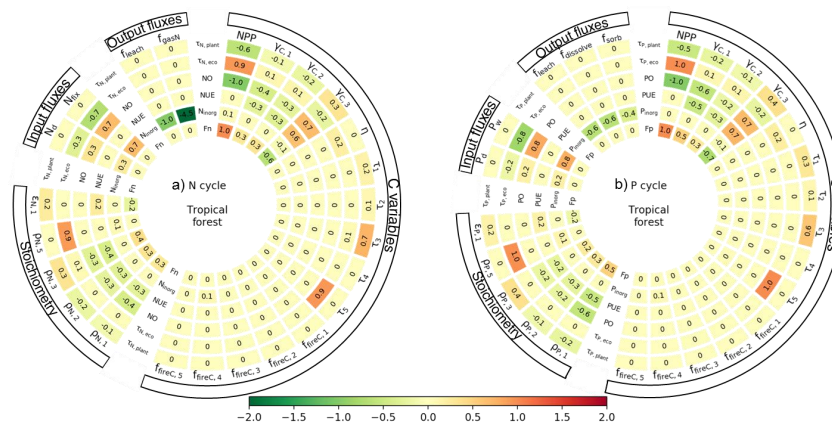
Figure 7 Mean sensitivity of the estimates of rates of nutrient uptake, inorganic nutrients, nutrient-use efficiencies, openness, turnover time of nutrients in the ecosystem and turnover time of nutrients in plants to the input variables for tropical forest. Results for other biomes are shown in Figs. S2 and S3.

1
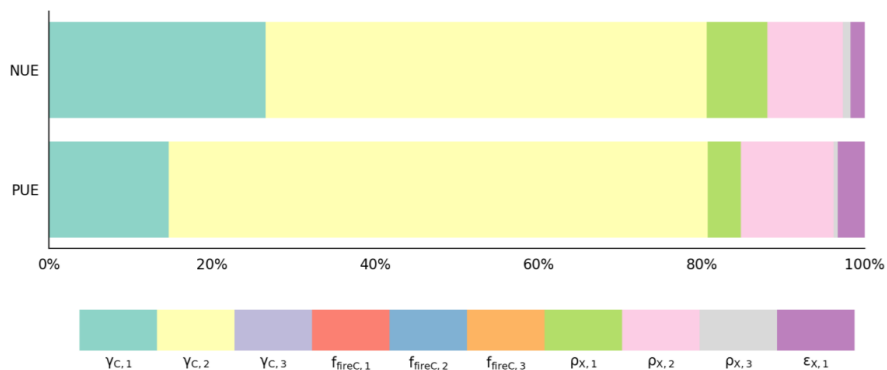
2 **Figure 8** Contribution of input data to the variance of the estimates of nutrient-use efficiencies ($X \in \{N,P\}$) for temperate

3 coniferous forests. $\gamma_{C, i=1,2,3}$ are NPP-allocation fractions to foliage, fine roots and wood, respectively. $f_{fireC, i=1,2,3}$ are fractions

4 of fire to total outgoing flux from foliage, fine roots and wood, respectively. $\rho_{x, i=1,2,3}$ ($X \in \{N,P\}$) are X:C ratios of foliage,

5 fine roots and wood, respectively. $\varepsilon_{X, 1}$ ($X \in \{N,P\}$) is the resorption coefficient of foliar nutrients.

6
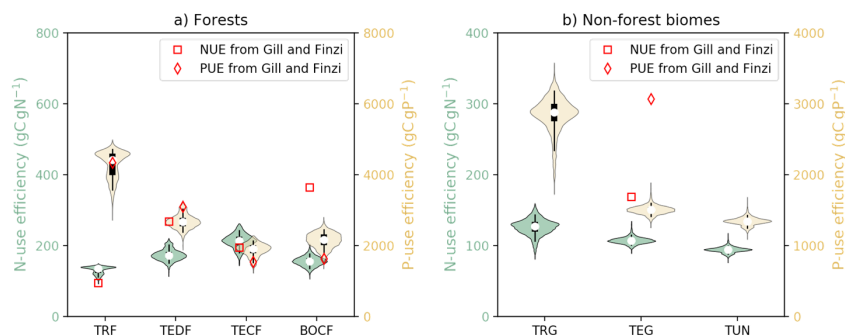
Figure 9 Violin plots of the nutrient-use efficiencies of the seven biomes from the experiment in which the allocation fraction of NPP to woody biomass and to leaves in coniferous forests is reduced. Open circles are the medians of all grid cells within each biome, with balloons representing the probability density distribution of each value. Black whiskers indicate interquartile (thick) and 95% confidence intervals (thin). The biomes are tropical rainforests (TRF), temperate deciduous forests (TEDF), temperate coniferous forests (TECF), boreal coniferous forests (BOCF), tropical/C4 grasslands (TRG), temperate/C3 grasslands (TEG) and tundra (TUN). The red squares (NUE) and diamonds (PUE) are the independent estimates from site observations and other generic data sets compiled and harmonized by Gill and Finzi (2016) based on site measurements of GPP and net N/P mineralization.